

**GRAPHENE-POLYIMIDE NANOCOMPOSITE PIEZORESISTIVE THIN FILM
DEVICE FOR STRAIN AND PRESSURE MEASUREMENT**

by

Shijing Luo

BS, Harbin Institute of Technology, China, 2014

Submitted to the Graduate Faculty of
Swanson School of Engineering in partial fulfillment
of the requirements for the degree of
Master of Science

University of Pittsburgh

2016

UNIVERSITY OF PITTSBURGH
SWANSON SCHOOL OF ENGINEERING

This thesis was presented

by

Shijing Luo

It was defended on

April 4, 2016

and approved by

Patrick Smolinski, Ph.D., Associate Professor

Department of Mechanical Engineering and Materials Science

Jung-kun Lee, Ph.D., Associate Professor

Department of Mechanical Engineering and Materials Science

Thesis Advisor: Qing-Ming Wang, Ph.D., Professor

Department of Mechanical Engineering and Materials Science

Copyright © by Shijing Luo

2016

GRAPHENE-POLYIMIDE NANOCOMPOSITE PIEZORESISTIVE THIN FILM DEVICES FOR STRAIN AND PRESSURE MEASUREMENT

Shijing Luo, M.S

University of Pittsburgh, 2016

In this thesis, piezoresistive thin film strain/pressure sensors made of graphene-polyimide (PI) nanocomposites with graphene concentration varies from 1.0wt% to 1.8wt% were fabricated, and their piezoresistive properties were characterized. The range of the graphene concentration is determined by percolation threshold theory, so the nanocomposites remain as semiconductors. The graphene-PI nanocomposites suspension were fabricated by blending method and was put into an ultrasonic water bath for a few hours to fully disperse the solution and avoid agglomeration of graphene nano-fillers. The graphene-PI nanocomposite thin film strain sensors were fabricated by depositing the suspensions on the polyimide substrate through a drop-on-demand piezoelectric inkjet printer, and electrodes were coated by sputter coater. The electrical impedance with respect to the strain that the nanocomposite thin films suffered under uniaxial tension and uniform pressure were monitored, and the gauge factor of these sensors under two experimental circumstances were calculated and compared. The respond of these strain sensor to pressure was also directly related. The temperature effect was evaluated, and the temperature coefficients of these graphene-PI nanocomposites devices were determined, also a feasible compensation method to eliminate the temperature effect was proposed. Finally, the most sensitive strain gauge represented by the largest gauge factor was found, proving that graphene-PI nanocomposites are superior materials than metals to fabricate high sensitive strain sensors, and inkjet printing technique is a desirable method to achieve this.

TABLE OF CONTENTS

PREFACE.....	XII
1.0 INTRODUCTION.....	1
1.1 INTRODUCTION.....	1
1.2 RESEARCH OBJECTIVE	4
2.0 RESEARCH BACKGROUND	5
2.1 STRAIN AND PRESSURE SENSOR.....	5
2.2 GRAPHENE-PI NANOCOMPOSITE AS PIEZORESISTIVE MATERIALS .	12
2.2.1 Electronic and mechanical properties of graphene	12
2.2.2 Piezoresistive materials	14
2.2.3 Graphene based polymer nanocomposites	15
2.2.4 Graphene-based sensors.....	15
2.3 DEVELOPMENT OF INK-JET PRINTING TECHNOLOGY	16
2.3.1 Continuous inkjet printing	17
2.3.2 Drop-on-demand.....	18
2.3.3 Drop formation	19
2.3.4 Application of inkjet printer as fabrication methods.....	20
3.0 DESIGN AND FABRICATION OF GRAPHENE-PI NANOCOMPOSITE STRAIN SENSORS.....	23
3.1 INTRODUCTION.....	23

3.2	THEORETICAL BACKGROUND	24
3.2.1	Strain gauge.....	24
3.2.2	Gauge factor and sensitivity	26
3.2.3	Piezoresistive effect.....	27
3.2.4	Percolation theory.....	29
3.2.5	Equivalent circuit	31
3.2.6	Barlow’s Formula and Hook’s Law.....	33
3.2.7	Testing methods	34
3.3	GEOMETRIC SHAPE DESIGN.....	35
3.3.1	Formula deduction	36
3.3.1.1	Trapezoid shape	36
3.3.1.2	Resistance of trapezoid	36
3.3.1.3	Sensitivity of the trapezoid resistors.....	37
3.3.1.4	Ring shape.....	38
3.3.1.5	The resistance of ring resistors	39
3.3.1.6	Sensitivity of the ring resistors.....	40
3.3.2	Conclusion and discussions.....	41
3.4	GRAPHENE-PI NANOCOMPOSITE FABRICATION.....	42
3.4.1	Graphene-PI nanocomposite suspension fabrication.....	43
3.4.2	Printing procedure	44
3.4.3	Strain gauge fabrication.....	50
4.0	PIEZORESISTIVE PROPERTY CHARACTERIZATION OF GRAPHENE-POLYIMIDE NANOCOMPOSITE	54
4.1	GRAPHENE-PI NANOCOMPOSITE RESPOND TO UNIAXIAL LOAD.....	54

4.1.1	Experiment Setup	54
4.1.2	Result and Discussions	56
4.2	GRAPHENE-POLYIMIDE NANOCOMPOSITE RESPOND TO PRESSURE	59
4.2.1	Experiment Setup	60
4.2.2	Results and discussions	62
4.3	CONCLUSION	67
4.3.1	Printing technique	67
4.3.2	Piezoresistivity characterized by tensile test and pressure test	68
5.0	NANOCOMPOSITE RESPOND TO TEMPERATURE	70
5.1	INTRODUCTION	70
5.2	TEMPERATURE COEFFICIENT FACTOR	70
5.3	EXPERIMENTAL STUDY	71
5.3.1	Experiment setup and procedure	71
5.3.2	Experiment results.....	72
5.3.3	Conclusion and discussions.....	73
6.0	CONCLUSION	76
6.1	PRINTING ADVANTAGES	76
6.2	GENERAL CONCLUSIONS	78
6.3	FUTURE WORKS	80
	BIBLIOGRAPHY	81

LIST OF TABLES

Table 3.1 Pulse shape parameters	47
Table 4.1 Table summary and error analysis of gauge factor.....	58
Table 4.2 Strain generated by pressure	65
Table 4.3 Gauge factor with different graphene concentration	66
Table 5.1 Normalized temperature coefficient at each graphene concentration.....	74
Table 6.1 Comparison of different thin film fabrication methods [57]	77

LIST OF FIGURES

Figure 2.1 Bonded gauge and its working principles	6
Figure 2.2 T-shape and rosette-shape strain gauges. (a) T-shape, (b) 45 °-rectangular, and (c) 60 °-delta.....	7
Figure 2.3 Rosette strain gauge constructions in (a) planar version and (b) stack version.....	8
Figure 2.4 Elastic elements for pressure sensors	9
Figure 2.5 Commercialized diaphragm strain gauges for pressure sensors [1]	9
Figure 2.6 Quarter-bridge strain gauge circuit.....	11
Figure 2.7 Other configuration of the Wheatstone bridge circuit.....	11
Figure 2.8 Graphene lattice structure.....	12
Figure 2.9 Tight-binding graphene electronic band structure model.....	13
Figure 2.10 inkjet printing technology map.....	17
Figure 2.11 Classification of piezoelectric inkjet printhead actuation principle [43].....	20
Figure 3.1 Tetragonal Conductor.....	25
Figure 3.2 Energy band.....	28
Figure 3.3 Tunneling for electron	29
Figure 3.4 Electrical conductivity vs. graphene concentration for the nanocomposites films measurement results.....	31
Figure 3.5 Cole-Cole plot	32

Figure 3.6 Equivalent circuit for graphene-PI nanocomposite	32
Figure 3.7 Trapezoid.....	36
Figure 3.8 Ring and sector shape.....	39
Figure 3.9 Sensitivity comparison of rectangular, trapezoid and ring shape CNT-PI nanocomposite sensors [57].....	41
Figure 3.10 Ink-jet print station	44
Figure 3.11 Drop monitor on the computer	45
Figure 3.12 Drop analysis results.....	45
Figure 3.13 Favorable drops formation	46
Figure 3.14 (a) Principle of pulse shapes used to fire jetting devices.....	47
Figure 3.15 Back pressure.....	48
Figure 3.16 (a) Rectangular printing pattern and (b) Printing procedure	50
Figure 3.17 Sputter coating mechanism.....	51
Figure 3.18 Masks for interdigitated and concentric circular electrodes.....	52
Figure 3.19 The specimen ready for coating	52
Figure 3.20 Cressington sputter coater	53
Figure 4.1 Rectangular nanocomposite thin film.....	55
Figure 4.2 Uniaxial testing equipment.....	55
Figure 4.3 Normalized resistance change vs strain in different graphene concentration	57
Figure 4.4 Gauge factor at each concentration	58
Figure 4.5 Pressure test equipment	60
Figure 4.6 Vessel for pressure test.....	61
Figure 4.7 Impedance of test sample with CNT concentration of 1.0wt%	62
Figure 4.8 Impedance of test sample with CNT concentration of 1.2wt%	63

Figure 4.9 Impedance of test sample with CNT concentration of 1.4wt%	63
Figure 4.10 Impedance of test sample with CNT concentration of 1.6wt%	64
Figure 4.11 Impedance of test sample with CNT concentration of 1.8wt%	64
Figure 4.12 Resistance change with strain and gauge factor	66
Figure 4.13 Gauge factor with different graphene concentration	67
Figure 5.1 Samples placed on hotplate	72
Figure 5.2 Resistance change with respect to temperature	74
Figure 6.1 Drops of the sample under microscope [57].....	78

PREFACE

I am very grateful for having this opportunity to conduct this research, and I would like to express my sincerest appreciation to my thesis advisor, Dr. Qing-Ming Wang, for giving me this opportunity to work on this topic and for his guidance, encouragement, and support in this work and over the past two years of my M.S. study. I am very thankful to Dr. Patrick Smolinski and Dr. Jung-kun Lee for their kindly willingness to serve as my committee members and their helpful suggestions.

Meanwhile, I would like to thank my colleagues: Qiuyan Li, Huiyan Wu and Hongfei Zu, and for their help in my research, and all the other colleagues in my lab. I would also thank my boyfriend for his encouragement.

Finally, I would like to express my deepest gratitude to my families who are always supporting me and loving me.

1.0 INTRODUCTION

1.1 INTRODUCTION

A lot of physical quantities such as position, stress, temperature, pressure and humidity can be measured by another measurable event based on some physical or chemical principles. The device which can accomplish this change from a physical quantity of interest to a detectable physical parameter is called sensor [1] . One of the most common sensors is strain sensor which can indirectly measure force, and pressure according to basic mechanical principles.

Strain Sensors, which are made of diverse materials, have various applications in civil, industrial, medical, aerospace and many other engineering fields for strain estimation and monitoring [2] . One of its most prevalent usages is to detect the presence of structure damages in critical infrastructure. In practical, resistance changes when the material is under strain, which can be suggested by Poisson effect that the length and the cross-sectional area change when the material is under strain, and the definition of resistance of material $R = \rho (L/A)$, where ρ is the resistivity, L is the length, and A is the average cross-sectional area of the material, which implies that resistance varies with its length and cross section area. This effect that electrical resistance changes when the mechanical strain is applied is called piezoresistivity.

Conventionally, the techniques to characterize strain or displacement response in a mechanical structure can be categorized to non-contact and contact methods [3]. Typical non-

contact methods are laser strain micrometry and optical microscope. Laser strain micrometry employ two laser beams to focus on the opposite faces of the sample to measure out-of-plane strain [4], and to focus on the same face to obtain the interference speckles to further determine the in-plane strain response [5][6]. The measurement results are very accurate if the laser beam is aligned properly and the measured surfaces are of high quality. However, a laser instrument is usually awfully complicated and expensive, and often requires delicate laboratory conditions [6]. In the case of an optical microscope, it can only be used under low-frequency strain because of limited resolution [4]. Contact methods include resistive strain gauge, differential capacitive strain gauge and linear variable differential transformer (LVDT) [2]. The differential capacitive strain gauge measures the output voltage of two differential parallel plate capacitors, and the LVDT measures the output voltage of two differential transformers, both use the voltage output to reflect the structure displacement change. However, complex circuit requirements and sensitivity to vibration limit these two techniques usage in practical sometimes. Therefore, electric resistance strain gauge becomes the most common transducer to measure strain. This method is very convenient for large structures. Adhesives are employed to directly attach the resistance strain gauge to the host mechanical component, when under loads, the strain gauge deforms along with the host component, and the strain of the component can thus be determined accurately by measuring resistance change of the gauge [7]. However, the size of the strain sensor and even the thickness of the adhesives can influence the behavior of small structures under test. As a result, even smaller strain sensors are desirable to minimize their effects to the structure.

Strain gauges are often made of metal film, or piezoresistive semiconductors such as single crystal silicon and polycrystalline silicon, to characterize static or dynamic strain

variations in mechanical structures [8][9]. A piece of metal film resistor or a piezoresistive device is usually sandwiched between two insulation layers to fabricate a strain gauge. Gauge factor for most metal strain gauges range from 2 to 5, and since metals are rigid, it is hard to measure small deformation with metal strain gauges [10]. Polymer-based piezoresistive nanocomposites, on the contrary, have shown better structural flexibility and higher gauge factor, and can be utilized in fabricating miniaturized devices. Therefore, piezoresistive nanocomposite strain gauge nowadays plays a critical role in tactile strain sensing and pressure testing.

Several methods have been introduced to produce nanocomposite thin films: manually painting by brush and chemical dropper was implemented to fabricate single wall carbon nanotube (swCNT)-polyimide nanocomposite thin film [10]; spin coating method was employed to make ZnO-polyimide nanocomposite thin film [2]; ink-jet printing method was introduced to manufacture thin-film transistor of swCNT. Among all those thin films fabricating methods, the ink-jet printing method possesses more advantages than the others, for example, it can deposit versatile thin films with accurate shapes and sizes, add scalability and can greatly reduce material waste, also can better ensure the uniformity of the thin films.

Graphene, one of the booming carbon-based material, has been proved with a lot of advantages, and it has surpassed many other carbon-based materials such as carbon-nanotubes for easy pattern formation, thermal conductivity, good mechanical properties, and optical transparency. Enormous efforts have been devoted to explore its applications in plenty of science and engineering fields [11-15]. However, not much study has been done to investigate its probability of producing electrical/mechanical devices for testing strain/stress or pressure.

1.2 RESEARCH OBJECTIVE

The objective of this thesis is to demonstrate the piezoresistivity of graphene-polyimide nanocomposites and prove that it is a desirable candidate for producing strain/pressure sensors. To accomplish these goals, three research tasks were conducted: the first is to fabricate graphene-polyimide nanocomposite thin film strain gauges, the second is to characterize the performance of these transducers when under loads or pressure, and the third one is to estimate the temperature effect on the strain gauge, find the temperature coefficient of this piezoresistive nanocomposite devices, and compensate the temperature effect.

In this thesis, different amount of graphene will be added into polyimide matrix to form polymer matrix nanocomposites suspension with different graphene concentration. And these nanocomposites suspension will be deposited on polyimide film substrate by ink-jet printing technique. This thesis will manifest ink-jet printing method is a viable processing method with plenty of advantages, such as stability and uniformity of the solution to manufacturing thin film transducers. Depending on the complexity of the application requirement, more precise definitions of the sensitivity of sensors with different shape will be made, then the piezoresistive property of these nanocomposites will be explored. Finally, the sensitivity of the graphene-PI nanocomposite strain/pressure sensor was obtained through tensile tests and pressure tests, and the gauge factor of this strain gauge made of these nanocomposites will be found. The possible temperature effect on the performance of the nanocomposite sensors was considered, and the compensation methods were proposed.

2.0 RESEARCH BACKGROUND

Strain/stress sensors have been developed for many decades, it is now widely used to detect the deformations or structural changes of all kinds of structures. Currently, using a strain gauge to measure strains is believed to be the fastest and easiest way. Therefore, through all these decades, scientists have been making an endeavor to invent favorable strain gauge with high sensitivity. In this chapter, the history of strain gauge will be reviewed, as well as its principle. Among all kinds of materials, piezoresistive materials have exhibited superiority, and the piezoresistive properties of graphene-PI nanocomposites will be studied. Finally, the ink-jet printing methods used in this research to fabricate nanocomposite thin films will be elaborated.

2.1 STRAIN AND PRESSURE SENSOR

When a strip of some conductive material is stretched, it will become thinner and longer with the cross-section decreases, and it works the opposite way when the strip is under compressive stresses. Because the dependence of the conductors' physical property on its geometry, the strip can be used as a fundamental measuring element for physical force [16], such device is called electrical resistance strain gauge. The strain gauge can be used to infer the amount of applied force by measuring its resistance. Moreover, it can also be applied to produce a variety of types of sensors, such as pressure sensors, load cells, torque sensors, position sensors, etc. [1]. It was

first invented by Edward E. Simmons and Arthur C. Ruge in 1938 [17][18]. A strain gauge often consists a strain sensitive thin film made of metal or semiconductor material and an insulating backing carrier of the thin film, it can be available in various shapes and sizes to suit different applications.

Strain gauges are frequently used in mechanical engineering research and manufactory industries, they are usually smaller than a postage stamp, and the conductive materials are very thin, for example, a strain gauge made of round wire is about 1/1000 inch in diameter. Traditional strain gauge usually use metallic materials, the active part is the bonded zigzag grid of thin foil forming loops on the insulant carrier, it can store the deformation information of the strain gauge in the active grid length direction. Figure 2.1 shows the bonded strain gauge as well as its working principles: suffering uniaxial extension, the foil grid is elongated and its cross-section narrowed, causing an increase of the resistance; while under compression in the active length direction, the grid becomes broader and short, causing a decrease in the resistance [19].

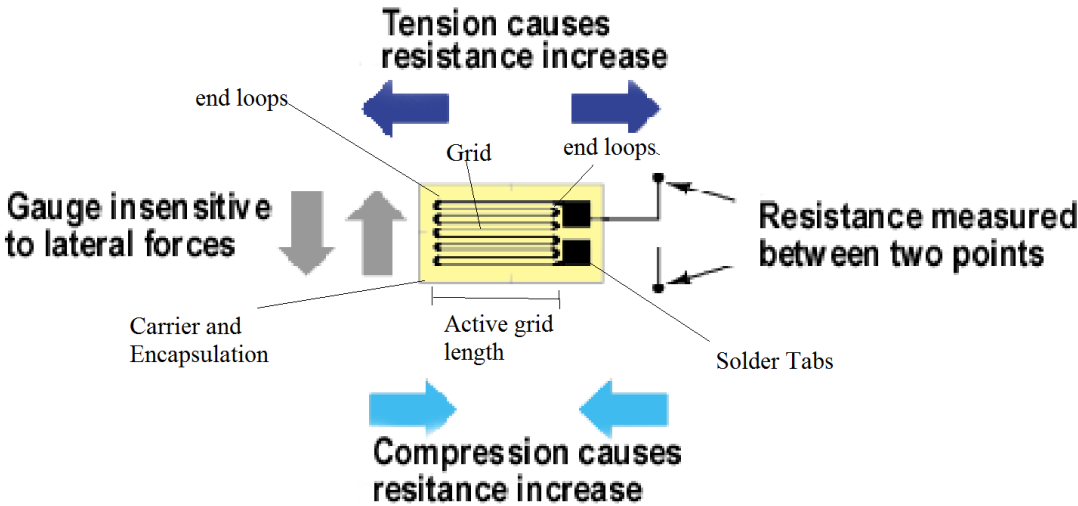


Figure 2.1 Bonded gauge and its working principles

From the above statement, it is not difficult to conclude that the orientation of the active grid will affect the accuracy of the strain measurement. The resistance change is sensitive if the force is uniaxial and is along suitable direction, so it is better to know the principal axes of the stresses at the testing points. Otherwise, the resistance change could not reflect the strain/stress amplitude exactly, and can even cause large error. Since the principal axes of the stresses are often difficult to pre-determined, to meet the urge demand of strain/stress/pressure measurement for complex structures, several different configurations of strain gauge have been designed to overcome the limitation of the single strain gauge. Prevalently, multiple ones are organized in certain pattern, like T-shape strain gauge for biaxial stress state, rosette-shape strain gauge for strain in different orientations and diaphragm strain gauge for pressure measurement. T-shape and rosette –shape strain gauge configurations are shown in Figure 2.2 (a) (b) (c).

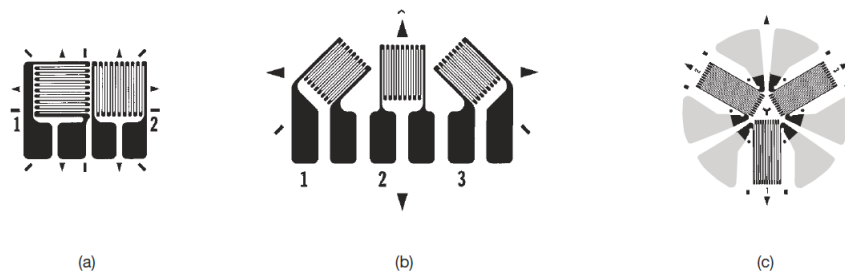


Figure 2.2 T-shape and rosette-shape strain gauges. (a) T-shape, (b) 45 °-rectangular, and (c) 60 °-delta

The T-shape strain gauge is made of two single strain gauge elements placed perpendicularly to each other, and can be applied to those situations where principal strain orientation is pre-known, typical examples are cylindrical pressure vessels and shafts on torsion. The rosette-shape strain gauge has wider implementation and can be employed in the situation where principal directions are uncertain. It measure strain on the surface in three directions, by strain-stress relationship in mechanics of materials, the principal strains and principal stresses

can be calculated out. For calculation convenience, the rosette is often made with 45 degrees or 60 degrees, as shown in Figure 2.2 (b) and (c). Those elements to construct a rosette strain gauge can be manufactured in either planar version or stack version, as shown in Figure 2.3, depending on where to apply. Panar construction gives smaller reinforcing effect and better heat dissipation to the test part while stacked construction can be installed on small spaces where its planar counterpart couldn't fit in.

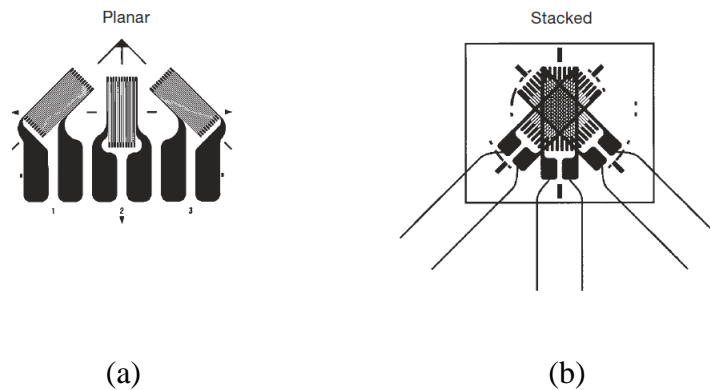


Figure 2.3 Rosette strain gauge constructions in (a) planar version and (b) stack version

A pressure sensor is a device that can convert pressure to mechanical or electrical signals [1], it often contains a primary sensor and a secondary sensor. The primary sensor is an elastic element which deforms under pressure, and some common elastic elements are shown in Figure 2.4, (a) is a Bourdon tube, it is made of a curved metal tube with an elliptical cross section which deforms when the pressure difference occurs the outside and inside the tube; (b) is the bellows and (c) is the capsule sensing elements, both are thin walled flexible metal tubes whose length changes when difference between external and internal pressure alters; (d) is a diaphragm sensing element, it is a thin elastic circular plate supported about its circumference, and the pressure difference will be proportionally reflected on the deformation of the diaphragm. The secondary elements convert the deflection information of the elastic elements into measurable

mechanical or electrical signals, for instance electrical voltage or mechanical rotation. Typical secondary element is made of strain gauge elements, capacitance elements and piezoelectric elements. Different types of these elements are employed in different situations, a strain gauge can be bonded directly on the diaphragm, while capacitance elements can be created when a fixed metal plate is placed above or below a metallic diaphragm, and piezoelectric crystal elements are effective elements for dynamic pressure measurement. Figure 2.5 shows two commercialized patterns of strain gauge diaphragm for pressure sensing.

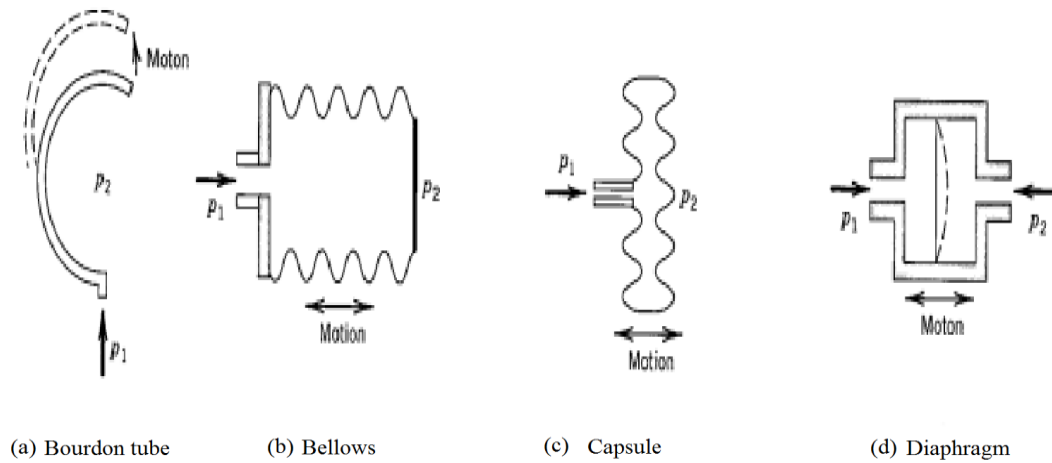


Figure 2.4 Elastic elements for pressure sensors

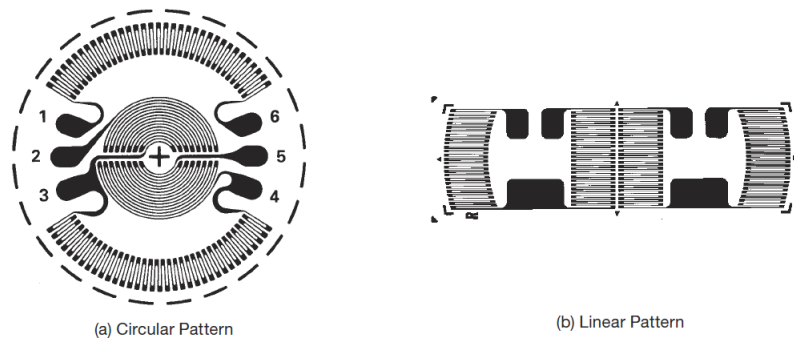


Figure 2.5 Commercialized diaphragm strain gauges for pressure sensors [1]

Traditional strain gauge resistances range from 30 Ohms to 3 kOhms when unstressed. This resistance may change only a little for the full force range of the gauge. Given the

limitations imposed by the elasticity of the gauge material and the backing material, it is very possible that forces great enough to induce large resistance change for measurement would cause permanent plastic deformation to the specimen, and disable the gauge to be a measurement instrument. In order to bring it to practical, the resistance must be measured in a small range with high accuracy.

To meet this precision demand, a bridge measurement circuit is introduced. Wheatstone bridge is a primary one. It consists four resistors forming a loop, the unknown component, which in this case is the strain gauge, is sit on one leg of the bridge, and its value will be measured by balancing other two legs of the bridge. Input voltage is applied across two junctions and the output voltage the other two junctions. The output voltage changes when the resistance of the strain gauge changes, so the amount of resistance change and the amplitude of strain can be derived from the voltage change. The strain gauge acts as a potentiometer whose resistance changes under stresses. Setting the rheostat arm of the bridge (in Figure 2.6 is R_2) equal to the initial strain gauge resistance, the bridge circuit will balance systematically and the voltmeter suggests zero. Applying tensile or compressive forces, the resistance of the strain gauge changes, causing unbalance of the bridge, and an indication occurs on the voltmeter. New resistance value

can be calculated by $V_G = \left(\frac{R_3}{R_1 + R_3} - \frac{R_x}{R_x + R_2} \right) V_{input}$, where V_G is the voltage on the voltmeter,

V_{input} is the input voltage, R_x is the new resistance value of the strain gauge. The Wheatstone bridge contains a single gauge is called quarter bridge, which is the simplest one, as shown in Figure 2.6. When connecting to two active gauge and four active gauge, the circuit is called half bridge and full bridge respectively, as shown in Figure 2.7. The advantage of the half-bridge and full-bridge circuit is to grant higher sensitivity over the quarter-bridge, and eliminate the

temperature effect. The disadvantage is that there is often not enough space to bond the complementary pairs of strain gauges, therefore, quarter-bridge is still the most frequently used one [19].

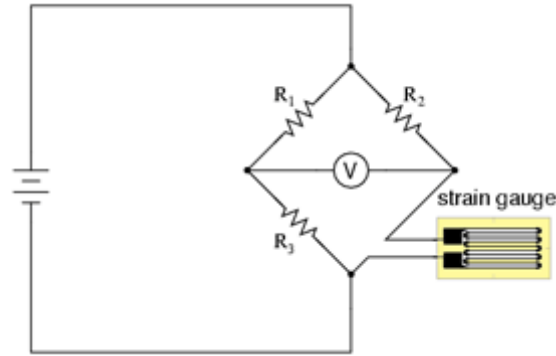
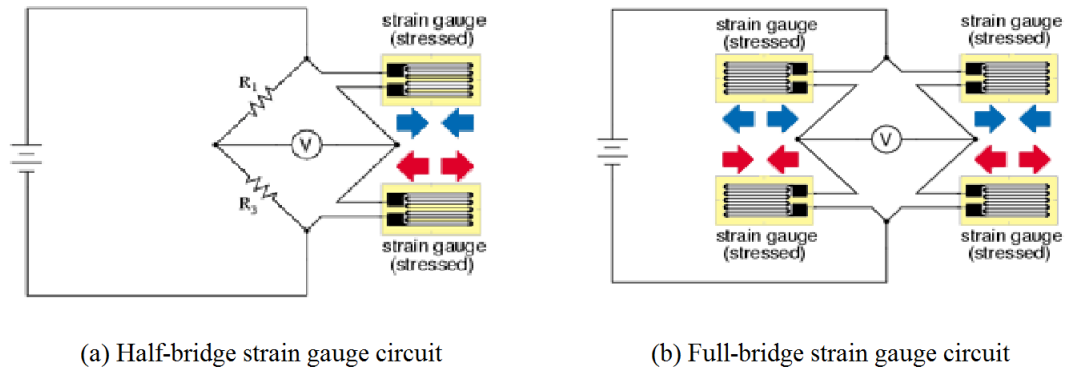


Figure 2.6 Quarter-bridge strain gauge circuit



(a) Half-bridge strain gauge circuit

(b) Full-bridge strain gauge circuit

Figure 2.7 Other configuration of the Wheatstone bridge circuit

For traditional metallic strain gauge, its resistivity change (of the order of 0.3) is small compared with that of semiconductors. Therefore its gauge factor, which is a common figure to indicate the sensitivity of electrical shift to mechanical deformation, is badly limited. Semiconductors, on the contrary, show higher resistance, more flexibility, longer fatigue life, and lower hysteresis under certain conditions, thus it has attracted vast attention of scientists to apply it into sensors. As piezoresistive semiconductors, graphene-polymer nanocomposites have been

studied and they exhibit superior mechanical properties as well as improved electrical conductivity over neat polymer or conventional graphite based composites [20]. In this thesis, graphene-polyimide nanocomposites are created to produce strain gauge.

2.2 GRAPHENE-PI NANOCOMPOSITE AS PIEZORESISTIVE MATERIALS

2.2.1 Electronic and mechanical properties of graphene

Graphene was first discovered by a physics professor Andre Geim and Konstantin Novoselov at the University of Manchester, it is a two-dimensional material which is isolated from graphite with only one atom-thick layer of carbon. The microstructure of graphene is densely packed by sp^2 hybridized carbon atoms to form a hexagonal structure, like a honeycomb. If rolling up, it can form zero-dimensional fullerene and one-dimensional carbon-nanotube (CNT). The carrier dynamics is strictly constrained in a 2D layer by reason of its high symmetric structure. There are two equivalent lattice sites A and B on the hexagonal lattice, as shown in Figure 2.8, which results in special electron hopping.

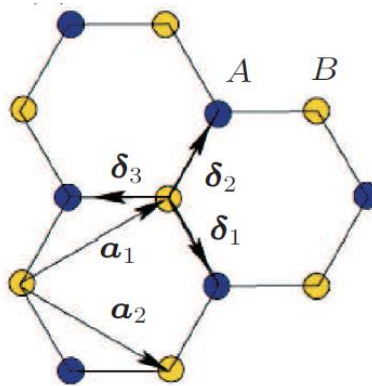


Figure 2.8 Graphene lattice structure

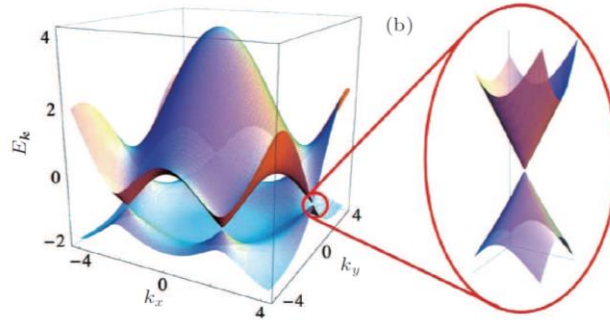


Figure 2.9 Tight-binding graphene electronic band structure model

Figure 2.9 shows the tight-binding electronic band model for monolayer graphene, the valence and conduction bands of graphene are conical valleys that touch at the Dirac points K and K' in the Brillouin zone. Near the Dirac point, the carrier has a linear dispersion relation $E = \hbar v F k$, so it can be called the massless Dirac fermion. The velocity of electrons in graphene is about 106 m/s, which is about 1/300 of the velocity of light.

The bilayer graphene is also a zero band-gap semiconductor, however, its electronic dispersion is not linear near the Dirac point. The energy band of graphene with more than three layers is very complicated, where its conduction bands and valence bands get overlapped. Because of its special electronic band structure, graphene exhibit a series of interesting physical phenomena and special properties, such as ballistic transport, ultrahigh mobility and anomalous quantum Hall Effect [21], non-zero minimum quantum conductivity [22].

The ever-increasing interest in graphene is also because of its excellent mechanical properties. The Young's modulus of graphene is high as about $E=1.0$ TPa, , the Poisson's ratio is about 0.186, and the third-order elastic stiffness $D = -2.0$ Tpa, the intrinsic breaking strength is 130GPa at as high as around 25% strain, which is very remarkable among materials with high mechanical strength, probably the highest value ever be measured [23].

2.2.2 Piezoresistive materials

Single crystal silicon and polycrystalline silicon are the first transducer elements used in fabricating piezoresistive strain gauges. Later, polymer matrix nanocomposites become prevalent due to their structural flexibility and possibility of multiple function, and they fit in well for small strain and flexible sensing. A large piezoresistive effect has been detected in silicon nanowires [24], the piezoresistive properties of single crystalline and polycrystalline silicon nanowires were explored by K. Reck [25]. The electrical and mechanical properties of ZnO nanowires, single wall carbon nanotubes (swCNT) multiple walls carbon nanotubes (mwCNT) and CNT-polymer nanocomposites have been studied [26-28].

The widely used carbon nanofillers are swCNT [10] [29], mwCNT [33-35], carbon nanofibers [30], carbon nanoblacks [31] and graphene [32]. Common insulating polymer matrix are epoxy [33], PMMA [34], EMMA [35], PE [29] [35], and PI [2] [36] etc.. The piezoresistivity mainly depends on the nanofiller, the influence of the matrix on piezoresistivity is very small, but the type of polymer matrix affects the viscosity of the nanofiller polymer suspension, and would characterize the mixing and dispersing process [37]. A lot of work has been done on CNT-polymer nanocomposites strain sensors, for example, Loh et al made swCNT-PE with sensitivity of 0.1~0.8 [29], Kang et al reported mwCNT-PMMA has gauge factor of 5 with maximum strain of 0.15% [34], Hu et al reported the gauge factor of mwCNT-Epoxy can reach to 20~25 under maximum strain of 0.6% [33]. Besides, some researches show that the gauge factor of ZnO-PI could be as high as 100 [2]. Among different types of polymer matrix, Highly aromatic polyimide resins have high thermal stability ($>300\text{ }^{\circ}\text{C}$), high glass transition

temperature ($T_g > 200\text{ }^\circ\text{C}$), high tensile strength, low creep, excellent radiation shielding capability, flexibility, thus become an advantageous matrix.

2.2.3 Graphene based polymer nanocomposites

There are some studies show that graphene based polymer nanocomposites exhibit superior mechanical properties than that of neat polymer or conventional graphite based composites. The improvement in mechanical properties by graphene is greater than 100% [20], depends on the aspect ratio of the graphene filler. Another advantage is that graphene based polymer composites exhibits a several fold increase in electrical conductivity, this is attributed to the formation of conducting network by graphene sheets in the polymer matrix. Some other benefits are like high thermal stability, good barrier properties, the graphene-based polymer nanocomposites also showed good EMI shielding efficiency. Most significantly, graphene based polymer nanocomposites is a semiconductor, which makes it feasible to create strain sensor with high gauge factor.

2.2.4 Graphene-based sensors

Some research has been done about graphene based sensors, there are some different type of graphene-based strain sensors, such as graphene strain sensors based on structure deformation, graphene strain sensors with over connected graphene sheets, and graphene strain sensors based in tunneling effect between neighboring graphene sheets [38]. For the first type, Huang et al. demonstrated that the suspended graphene devices were homogeneous by in situ nanoindentation, while electrical measurements were carried out simultaneously [39] and they

found that even with a larger deformation, the device resistance changed little in the experiments and the gauge factor was about 1.9, which is close to the calculated one (about 2.4). The second type is come up with due to a mechanism that the strain respond of the graphene network depends on the contact resistance of adjacent sheets, once under forces, tensile or compressive, the overlap area of neighboring flakes becomes smaller or larger, which is reflected by the change of resistance. For the third type, the gauge factor can range from roughly 12 to hundred. Lee et al. [40] reported the piezoresistance response of graphene and the graphene based strain sensor with a gauge factor of 6.1. Fu et al. [41] also demonstrated a monolayer graphene based strain sensor with high sensitivity. The recent research of Yu's group found that the transferred graphene on PDMS grown by chemical vapor deposit (CVD) has a higher gauge factor about 151 [42].

However, little research has been done on making strain gauge with graphene-PI nanocomposites, but its excellent mechanical and electrical properties suggest it could be a desirable element to produce high sensitive strain gauge. And since graphene shows much higher conductivity than carbon nanotube, we'd expect that nanocomposites with graphene filler would exhibit much higher gauge factor.

2.3 DEVELOPMENT OF INK-JET PRINTING TECHNOLOGY

The first inkjet like device was invented by William Thomson in 1858, but the prosperity of this technology didn't come out until late 1950s [43]. Since then ink-jet printing has attracted a lot more attention for its becoming a manufacturing technology with applications in fields beyond its traditional usage of printing text, graphics, and product marking. The applications have

broaden into fields like fabrication of polymer electronic components, organic light-emitting diodes, ceramic components, microarrays for biological screening, organic thin film transistors, light-emitting diodes, solar cells, conductive structures, memory devices, sensors, and biological/pharmaceutical tasks [44] [45]. Several kinds of inkjet printing technology has been developed, and the classification is shown in Figure 2.10. Among them piezoelectric and thermal inkjet are the dominants in this field.

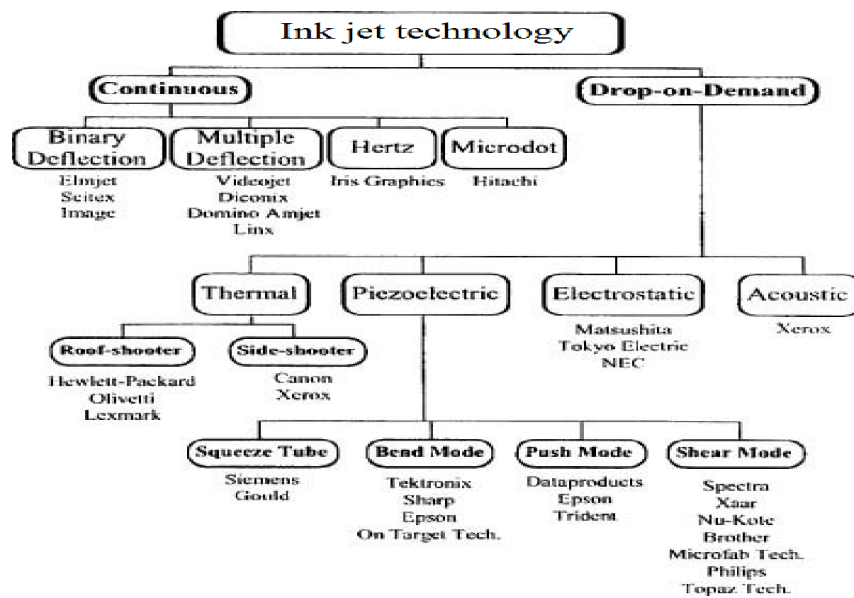


Figure 2.10 inkjet printing technology map

2.3.1 Continuous inkjet printing

Continuous Inkjet printing (CIJ) came out in early 1960s, and was elaborated for inkjet bar coding in Stanford University. The continuous inkjet (CIJ) method is used commercially for marking and coding of products and packages. In 1867 Lord Kelvin patented the syphon recorder, which recorded telegraph signals as a continuous trace on paper using an ink jet nozzle deflected by a magnetic coil. The first commercial devices (medical strip chart recorders) were

introduced in 1951 by Siemens.[46] In CIJ technology, a high-pressure pump directs liquid ink from a reservoir through a gunbody and a microscopic nozzle, creating a continuous stream of ink droplets. A piezoelectric crystal creates an acoustic wave as it vibrates within the gunbody and causes the stream of liquid to break into droplets at regular intervals, there is research indicates that tremendous drops may be achieved per second. The degree of the ink droplet deflection is controlled by a changeable electrostatic field created by a charging electrode as drops form. Charged droplets are separated by one or more uncharged "guard droplets" to minimize electrostatic repulsion between neighboring droplets. CIJ is one of the oldest ink jet technologies in use, the major advantages are the very high velocity (~20 m/s) of the ink droplets, which allows for a relatively long distance between the print head and the substrate, and the very high drop ejection frequency, allowing for very high speed printing [47]. Some companies like Sharp, IBM, Honeywell developed their own licensed technology with further development of multiple drop defection, increased drop frequency, and multi-jet printing [43].

2.3.2 Drop-on-demand

Unlike the CIJ create dsrops continuously, the drop-on-demand DOD creates drops only when an actual pulse is provided. The DOD technique is much more widely used than CIJ, and there is no need to use the complicated hardware for charging electrodes, deflecting electrodes and re-circulation system [43]. The most prevalent DOD techniques are thermal DOD and piezoelectric DOD. The ink is held in the nozzle by a negative pressure and by applying a high voltage pulse to the electrodes located outside the nozzle, a drop of ink is pulled out by the deflection of the nozzle [48].

The first idea of thermal inkjet printing is to generate boiling aqueous ink drop at certain time instances in 1960s. In 1979, Canon re-invented the DOD printhead called bubble jet which is

actuated by a water vapor bubble, and the droplet was ejected in a perpendicular direction from the evaporating bubble. At the same time, HP introduced its low cost inkjet printer called top shooter design with jetting direction in line with the evaporating bubble in 1984 [43]. The print cartridges consist of a series of tiny chambers, each containing a heater. A pulse of current is passed through the heating element causing a rapid vaporization of the ink in the chamber and forming a bubble, which causes a large pressure increase, propelling a droplet of ink. However, the inks must have a volatile component to form the vapor bubble.

Piezoelectric inkjet (PIJ) use a piezoelectric material instead of a heating element in an ink-filled chamber behind each nozzle. When a voltage is applied, the piezoelectric material deformed to generate a pressure pulse in the fluid, forcing a droplet of ink from the nozzle. Piezoelectric inkjet allows a wider variety of inks than thermal inkjet as there is no requirement for a volatile component, and no buildup of ink residue, but the print heads are more expensive [47]. There are several patents in 1970s and 1980s that contribute the development of this technology. First squeeze mode PIJ was proposed by Zoltan of Clevite Company in 1972 [49]. A bend mode of operation was used by Stemme of Chalmers University, the wall of the ink chamber is made of a diaphragm bonded with a piezoelectric ceramic which would bend under voltage in 1973 [50]. Kyser et al. patented similar bending mode PIJ with different shape of actuation plate in 1976 [51]. S. Howkins of Exxon in 1984 described the push mode operation where a piezoelectric element pushes against an ink chamber wall to deform the ink chamber and the electrical field is applied in the poling direction. Finally, the shear mode was proposed by Fischbeck [43].

2.3.3 Drop formation

This section will further elaborate the piezoelectric inkjet printer and different actuation principles. The driving force of a piezoelectric inkjet printhead is ‘inverse piezoelectric effect’,

meaning that the structure deforms when an external electric field is applied. As mentioned above there are three modes of actuation: push mode (also known as bump mode), bend mode and shear mode, as shown in Figure 2.11. The push mode has the actuator move along the polarization of the piezoelectric material, to deform an ink channel, the piezoelectric elements need to be supported by a substrate which supplies the reaction force. But the substrate would introduce mechanical stress and the piezoelectric behavior would be influenced. Bending mode actuators completely or partly bend the piezoelectric channel wall. In both bump mode and bend mode actuation, electric field is applied in the same direction as the polarization direction. Shear mode actuators use electric field applied perpendicular to the polarization direction which results in a shear deformation parallel to the polarization direction [43].

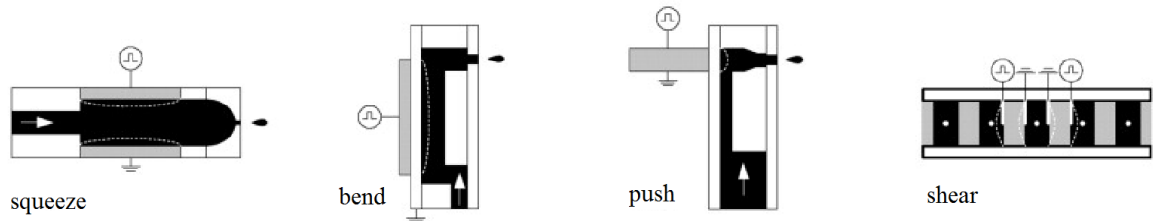


Figure 2.11 Classification of piezoelectric inkjet printhead actuation principle [43]

2.3.4 Application of inkjet printer as fabrication methods

Inkjet printing technique has been developed an important fabrication method to print text and images onto papers and other surfaces like cans and bottles [43]. Then, it has been developed to fabricate single layer or multiple-layer product, including electrical mechanical devices and circuits. Successful endeavors have been made to utilize inkjet printing technology to fabricate organic-nonorganic transistors, light-emitting diodes, ceramics, solar cells and biopolymer arrays [52]. Traditional deposition approaches involve a great deal of wasted materials, but result in a fairly

uniform deposition profiles over the substrate. By contrast, inkjet printing is an anisotropic (localized) deposition process, but it can obtain a layer uniform in overall scale, and it can make use of the materials with little waste, it does not require the use of shadow masks as it is a direct writing process.

Van Osch et al. DOD deposit conductive tracks on polymeric substrates by inkjet printing technique [53]. A silver ink with 20wt% silver nanoparticles suspended in ethylene glycol/ethanol mixture was inkjet printed on transparent polyarylate film performed by using a piezoelectric Dimatix DMP 2800 (Fuji film).

Singh et al.[54] demonstrated bright inkjet-printed OLEDs based on Ir-based phosphorescent macromolecules anchored on a polyhedral oligomeric silsesquioxane (POSS) molecular scaffolding used as a phosphorescent dye in a polymer ink containing a hole transporting polymer, poly(9-vinylcarbazole) (PVK) and an electron transporting polymer, 2-4-biphenyl-5-4-tertbutyl-phenyl-1,3,4-oxadiazole (PBD).

Inkjet printing can be used to deposit materials for inorganic and hybrid organic/inorganic solar cells. $\text{CuIn}_x\text{Ga}_{1-x}\text{Se}_2$ (CIGS) has been used as a material for high-efficiency solar cells [54]. Schubert and coworkers showed the effectiveness of using bulk heterojunction structures in inkjet-printed solar cells.

Many kinds of sensors have been made using inkjet printing methods, micro-electromechanical system (MEMS)-based sensors involve the deposition of functional layers to perform chemical and biochemical sensing tasks. Bietsch et al.[55] demonstrated the fabrication of nanoscale cantilever-based sensors using inkjet printing. SAM layers of alkanethiols were deposited on gold-coated cantilever structures. Panhuis et al.[56] used coiled conformation biopolymers to distribute SWCNTs and printed transparent composite films on a PET substrate.

In many other science and engineering fields, like biological and pharmaceutical and so many, inkjet printing technology has been showing its effectiveness and advantages. Inkjet printing offers resolutions in the micrometer range, and hence it is a potential technique for dispensing etching species, in applications like flat-panel displays [54]. In this thesis, ink-jet printing technique will also serve as a critical fabricating methods.

3.0 DESIGN AND FABRICATION OF GRAPHENE-PI NANOCOMPOSITE STRAIN SENSORS

3.1 INTRODUCTION

Piezoresistive materials have long been used as transducer elements for pressure and strain testing, because, in general, piezoresistive strain gauge exhibit a significantly higher larger gauge factor, which is the most common parameter used to determine the sensitivity of a strain sensor. The higher gauge factor demonstrates the higher sensitivity of a device. Thus, for many years, scientists have been searching hard for sensitive materials for strain sensors, among all the materials, semi-conductive materials become favorable candidates. As the study of the newly discovered material graphene getting wider and deeper, graphene nanocomposites attract scientists' attention to fabricating high sensitive strain sensor.

In this chapter, the concept of strain gauge and the definition of gauge factor will be explicitly explained, the piezoresistive effect will be introduced, followed by threshold theory, the electronic and piezoresistive properties, and mechanical properties of graphene will be studied. The background of graphene will be briefly reviewed, then the experiment setup and procedure will be demonstrated. The equivalent circuit of the nanocomposite transducer is presented, which not only represents the electrical property of the nanocomposite thin film but

also shows which parameters should be tested during the experimental study, to investigate the electrical properties of the nanocomposite.

Graphene polyimide nanocomposites with a series of different graphene weight ratio are fabricated. In order to acquire uniform graphene thin film, ink-jet printing method is applied to deposit the graphene polyimide nanocomposite suspension on a polyimide substrate. To investigate the piezoresistive properties of graphene nanocomposite through its impedance change, gold electrodes are coated on the substrate by utilizing shadow masks and a sputter coating system, the nanocomposite thin film is made lying across the middle of the electrodes. The sample will also be baked in the oven for a few hours to evaporate the solvent and get the nanocomposite fully cured. Thereupon, the sample can be used for testing.

3.2 THEORETICAL BACKGROUND

3.2.1 Strain gauge

The electrical resistance describes the difficulty to pass an electrical current through a conductor, it is affected by the physical property of the material and the shape of the object. For certain material, the resistivity is a constant. And for long thin conductors, it is assumed that the electrical current gets through with uniform density. The electrical resistance can be computed with

$$R = \rho \frac{l}{A} \quad (3.1)$$

Where ρ is the resistivity of the material, l is the length and A is the cross-section area of the conductive object. Figure 3.1 demonstrates the resistance of a tetragonal long thin conductor as an example.

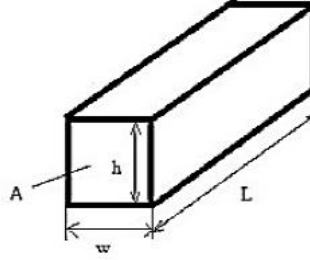


Figure 3.1 Tetragonal Conductor

Taking the natural logarithm on both sides of Equation (3.1),

$$\ln R = \ln \rho + \ln l - \ln A \quad (3.2)$$

Then take the derivative of Equation (3.2),

$$\frac{dR}{R} = \frac{d\rho}{\rho} + \frac{dl}{l} - \frac{dA}{A} \quad (3.3)$$

Substitute A with $A = wh$, which is the area of the cross-section area,

$$\frac{dA}{A} = \frac{w \cdot dh + h \cdot dw}{w \cdot h} = \frac{dh}{h} + \frac{dw}{w} \quad (3.4)$$

Given the definition of Poisson's ratio,

$$\nu = \frac{d\varepsilon_{transsection}}{d\varepsilon_{axial}} \quad (3.5)$$

We have

$$\frac{dh}{h} = \frac{dw}{w} = -\nu \frac{dl}{l} \quad (3.6)$$

Along with the definition of strain, $dh/h = dw/w = \varepsilon_{transsection}$, $dl/l = \varepsilon_{axial}$, we have

$$\frac{dA}{A} = -2\nu \frac{dl}{l} = -2\nu \varepsilon_{axial} \quad (3.7)$$

Substitute Equation (3.7) into Equation (3.3), we derive

$$\frac{dR}{R} = \frac{d\rho}{\rho} + (1+2\nu)\varepsilon_{axial} \quad (3.8)$$

Rewrite the Equation (3.8) by dividing ε_{axial} on both sides, we get

$$\frac{\frac{dR}{R}}{\varepsilon_{axial}} = \frac{\frac{d\rho}{\rho}}{\varepsilon_{axial}} + (1+2\nu) \quad (3.9)$$

Where the left term of the Equation (3.9) is the gauge factor, which is the main factor we concerned and will be specifically elaborate afterward. On the right side, the first term describes the piezoresistive property of the material, while the second term in the parentheses reveals that the resistivity varies with strain.

3.2.2 Gauge factor and sensitivity

The most common parameter to measure the sensitivity of strain gauge is the gauge factor, it characterizes the normalized resistance change compared to strain, and is defined as

$$GF = \frac{dR/R}{\varepsilon_{axial}} \quad (3.10)$$

From the definition, the larger the gauge factor is, the greater the electric signal indicated by resistance changes with small strain, so large gauge factor is preferred. Meanwhile, the gauge

factor of certain material is constant, which makes it a good candidate to represent the sensitivity of the strain sensor.

In general, the gauge factor of metallic strain gauges is dominated by the geometry term, while for piezoresistive strain gauges, the gauge factor is more dependent on the first term of Equation (3.9) [57]. Define it as a longitudinal piezoresistive coefficient, written as γ_l .

$$\gamma_l = \frac{\frac{d\rho}{\rho}}{\varepsilon_{axial}} \quad (3.11)$$

For semiconductors, the longitudinal piezoresistive coefficient γ_l can be several orders larger than the resistance change under deformation, in silicon and germanium, it can be 50 to 100. For this reason, semiconductor has become attractive materials to fabricate strain gauge and has acquired satisfactory results in many ways.

During the test, the deformation is very small, and both the geometry term and the piezoresistive effect can be regard as constants. Thus, the resistance change along with strain exhibit a linear relationship, which is represented by gauge factor (GF) in this research.

3.2.3 Piezoresistive effect

To explain the piezoresistive effect, we can take a look at the molecular scale. One of the main reason is the bandgap in the semiconductor. The states of an electron in metal (conductor) are different with that in semiconductor and insulator. In metal, the second Brillouin Zone (BZ) is overlapped with the first BZ, as shown in Figure 3.2 (a), bands overlap and eliminate the energy gaps. In semiconductor or insulator, the overlapping of the energy band cannot cover the

entire energy gap, so there is still energy gap exists in the whole scale, as indicated in Figure 3.2 (b), which will prevent electrons from getting through.

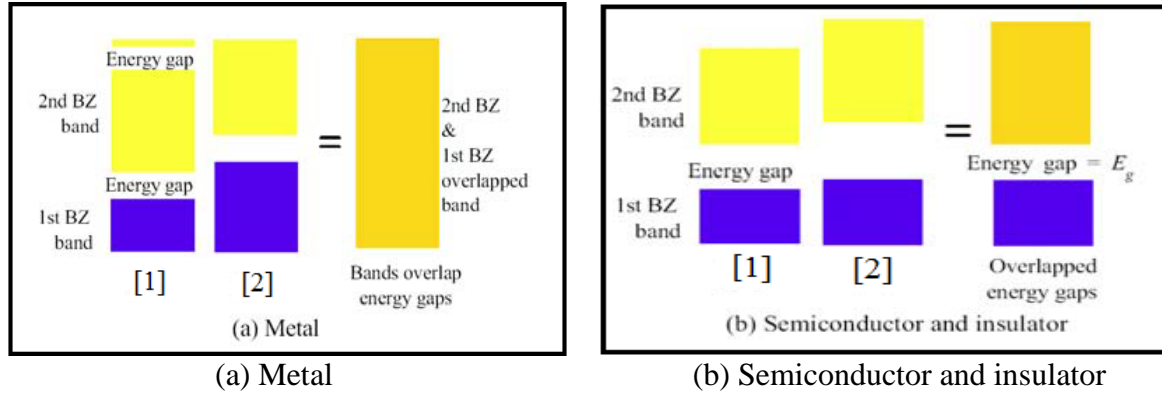


Figure 3.2 Energy band

Because of the energy band gap, the inter-atomic distance change will result in the change of electron mobility into conduction band when the material is subjected to force and strain arises. In a macroscopic view, the resistivity changes. Briefly, when the material is under tensile force, the distance between atomics increases, it becomes harder for an electron to jump into the conduction band, and the resistance goes up, verse vice, when the semiconductor is compressed, the inter-atomic distance decreases, and the resistance will reduce.

Another significant reason is the tunneling effect in the semiconductor. According to Quantum theory, there is a chance for an electron to tunneling (leaking) through the potential energy barrier V_0 , Figure 3.3 shows the wavefunction for electron incident on a potential energy barrier, the wavefunction decays in region II because the energy of the electron is less than the potential barrier.

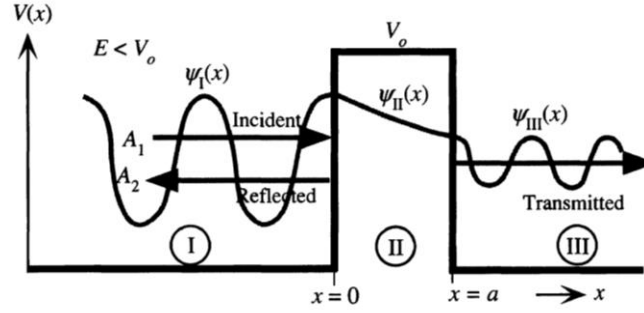


Figure 3.3 Tunneling for electron

When the force is applied to graphene nanocomposite thin film, under uniaxial tensile test for example, the distance between graphene molecules increases, it could add difficulty for tunneling happening, which leads to tunneling resistance increases, thus, the overall resistance goes up. The resistance evoked by tunneling can be approximated by

$$R_{tunnel} = \frac{V}{AJ} = \frac{h^2 d}{Ae^2 \sqrt{2m\lambda}} \exp\left(\frac{4\pi d \sqrt{2m\lambda}}{h}\right) \quad (3.12)$$

Where respectively R_{tunnel} —tunneling resistance, J—tunneling current density, V—electrical potential difference, e—the quantum of electricity, m—mass of the electron, h—Planck's constant, d—the distance between graphene molecules, λ —the height of barrier and A—cross section of the tunnel.

3.2.4 Percolation theory

According to the percolation theory, the conductivity of composite materials made up of a polymeric matrix and conductive fillers is affected by the concentration of the filler. The insulator transit to conductor as the conductive filler fraction rises in a small range, this critical value of concentration is defined as percolation threshold. Below the percolation threshold, the

probability of forming a conducting path approaches to infinitely, the composite behaves like an electrical insulators. Upon rising the filler concentration, the neighboring particles get close or even contacted, forming a conductive path in a small local area. When the local conductive paths are enough to cross the whole composite thickness, an effective conductive path is formed, causing a sharp increase of the bulk electrical conductivity of the material, so the composite becomes conductor beyond the threshold. [58] The critical concentration can be represented by

$$\sigma = c(x - x_{critical})^t \quad (3.13)$$

Where σ is the conductivity, c is a constant, x is the concentration of graphene, and the critical concentration value indicate the percolation threshold, at which a large conductivity (σ) varies with small concentration variations, t is the critical exponent that determines the trend of the function around the critical concentration.

To serve as semiconductor and obtain largest gauge factor, the concentration of graphene at the percolation threshold is the favorable. At this point, the change in resistivity with strain is dominated by large changes in the resistivity, resulting in larger gauge factors. The conductivity and concentration relationship curve is plot in Figure 3.4, which shows that the percolation threshold of graphene-PI nanocomposite is between 0.6wt% to 1.8wt%. Accordingly, in this research, the nanocomposite with graphene concentration from 1.0wt% to 1.8wt% with a step size of 0.2wt% was studied, as well as the electrical properties of the samples with each graphene weight ratio.

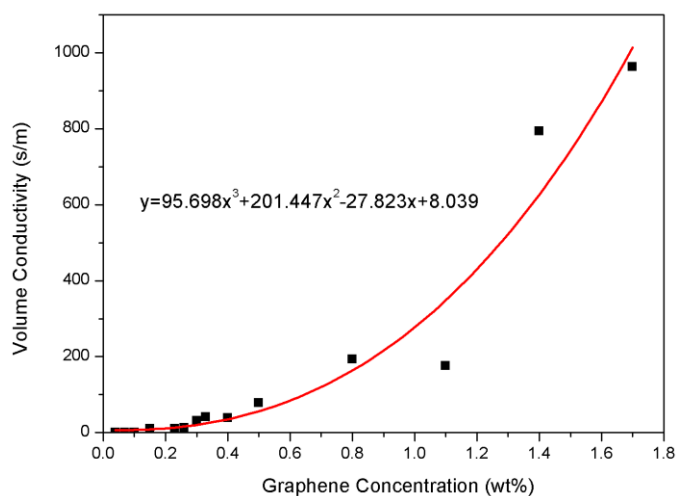


Figure 3.4 Electrical conductivity vs. graphene concentration for the nanocomposites films measurement results

3.2.5 Equivalent circuit

Electrical impedance spectroscopy (EIS) characterizes the frequency response of the impedance and provides important structure-property relationships of the device, guiding the material design and the device application. The impedance spectra data from the electrical impedance spectroscopy yields a semi-circle in the complex plot between real and imaginary parts of the nanocomposite impedance. This plot is called the Cole-Cole plot, as shown in Figure 3.5

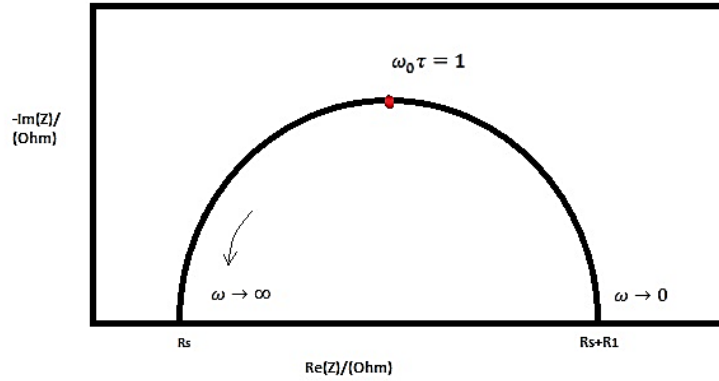


Figure 3.5 Cole-Cole plot

Data analysis of EIS requires modeling of the nanocomposites which can be represented by their representation as equivalent electrical circuit. The equivalent circuit for the graphene-PI nanocomposite can be established as a parallel connection of a resistance and a capacitor connect with another resistor in series, as shown in Figure 3.6.

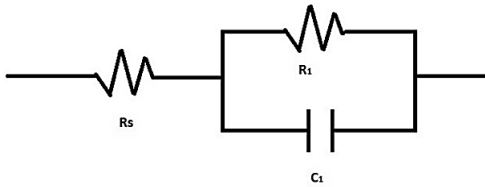


Figure 3.6 Equivalent circuit for graphene-PI nanocomposite

The impedance of this model is derived in Cartesian form, given as $Z = R + jX$, where R is the real part (resistance), and X is the imaginary part (reactance). Also, the impedance of resistance and capacitor are given as $Z = R$ and $Z = \frac{1}{j\omega C}$, respectively.

From the equivalent circuit, the total impedance of the nanocomposite thin film Z is as following:

$$\begin{aligned}
Z &= R_s + \frac{1}{\frac{1}{R_1} + j\omega C_1} \\
&= R_s + \frac{R_1}{1 + j\omega R_1 C_1} && \text{where } j^2 = -1 \\
&= R_s + \frac{R_1(1 - j\omega R_1 C_1)}{1 - (j\omega R_1 C_1)^2} \\
&= \left(R_s + \frac{R_1}{1 + \omega^2 R_1^2 C_1^2}\right) - j \frac{\omega R_1^2 C_1}{1 + \omega^2 R_1^2 C_1^2} \tag{3.14}
\end{aligned}$$

The R-X relationship is a semi-circle when frequency goes from zero to infinity, as the Cole-Cole plot shown in Figure 3.5, when $\omega \rightarrow 0$, the impedance is $Z = R_s + R_1$, it is the summation of the series resistance and the parallel resistance to the capacitance, which changes with the content of graphene concentration in the nanocomposites. While when $\omega \rightarrow \infty$, the impedance $Z = R_s$ [2]. the series resistance, represented by the minimum of $\text{Re}(Z)$ value of the semicircle, is negligible for these nanocomposites, which indicates that the electrodes and the nanocomposites have a negligible contact resistance. At the maximum $\text{Im}(Z)$, $\omega_0 \tau = \omega_0 RC = 1$, so at the top point of the semicircle, $\omega_0 = \frac{1}{RC}$, where C is the equivalent capacitance and τ is the time constant of the material.

3.2.6 Barlow's Formula and Hook's Law

Hook's Law is introduced for uniaxial tensile test, it gives the linear relationship between stress and strain:

$$\sigma = E \cdot \varepsilon \tag{3.15}$$

Where E is the Young's modulus, and it is 2.5GPa (362600psi) for the polyimide substrate utilized in this research.

Barlow's Formula is introduced to conduct pressure test in the vessel, it relate the internal pressure to the dimension of the pipe and the reacting stress on the substrate.

$$P = \frac{2\sigma t}{d \cdot SF} \quad (3.16)$$

Where P stands for pressure, σ is the stress, t is the thickness of the substrate, d is the inner diameter of the vessel, and SF s the safety factor, which is generally 1.5 to 10. In this research, the thickness of the polyimide thin film is $t = 0.005$ inches. The diameter of the pressure vessel is 2 inches. The safety factor is chosen as 1.5 in this thesis.

3.2.7 Testing methods

To investigate the piezoresistive property of the graphene-polyimide nanocomposite, strain needs to be generated and the corresponding resistances have to be measured. Simple uniform strain can be generated through tensile test with uniaxial force, static or dynamic strain can be generated by cantilever beam, and strain along radius directions can be generated by applying pressure on the diaphragm in a pressure vessel. In this thesis, uniaxial tensile test and vessel pressure test are conducted.

To study the electrical property of the graphene-PI nanocomposite, the simultaneous resistance and impedance will be measured when the material is under strain. The electrical impedance spectroscopy (EIS) measurement is achieved by using an impedance analyzer so the real imaginary part of the impedance as well as the capacity will be obtained. Although the impedance can already measure the resistance, it can capture the impedance only at specific

times at a frequency roughly from zero to infinity. In order to directly read the resistance and observe the resistance change with increasing strain in a continuously time period a DC current/voltage source measure unit will also be utilized in the tensile test.

3.3 GEOMETRIC SHAPE DESIGN

In previous chapters, we have made our goal of fabricating graphene-PI nanocomposites with ink-jet printing technology, so the shape and size of the strain sensitive material can be accurately controlled. In this chapter, the geometry effect will be theoretically discussed, and graphene-PI nanocomposites thin film with suitable shape will be designed for different applications, in this thesis, they are used for uniaxial tensile test and static pressure test.

For metallic strain gauges, the effective materials are often made in loop-like shape. However, the strain responds of piezoresistive materials to external forces are much more obvious, and the reacting resistance changes dramatically, so it is not necessary to fabricate piezoresistive strain gauge in loop-shape. But still, for different application, the geometric shape of the strain gauge may affect the sensitivity and accuracy. For uniaxial tensile test, the strain along the elongation direction is much significant than that along width direction, thus the simple rectangular films can fully reflect the deformation under uniaxial stresses. For vessel pressure test, the strain along different orientations can be affected. As a result, the trapezoid shape and the ring shape were proposed.

3.3.1 Formula deduction

3.3.1.1 Trapezoid shape

If the width of the quadrangle on two parallel sides do not share the equal length, the quadrangle is a trapezoid, as shown in Figure 3.7.

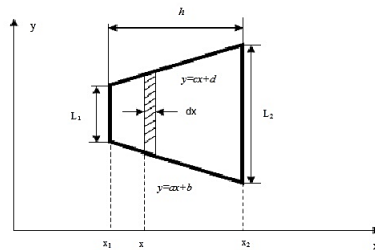


Figure 3.7 Trapezoid

3.3.1.2 Resistance of trapezoid

The resistance of the trapezoid cannot simply be derived by the general definition of resistance,

which is $R = \rho \frac{l}{A}$. However, the very narrow strip on the trapezoid can be taken as a rectangle

whose resistance can be derived by $R = \rho \frac{l}{A}$. For the narrow strip, the resistance can be

expressed as:

$$dR = \rho \frac{dx}{[(c-a)x + (d-b)]t} \quad (3.17)$$

Integrate the above equation to derive the resistance in the whole scale

$$\begin{aligned}
R &= \int_{x_1}^{x_2} \rho \frac{dx}{[(c-a)x + (d-b)]t} \\
&= \frac{\rho}{(c-a)t} \ln[(c-a)x + (d-b)] \Big|_{x_1}^{x_2} \\
&= \frac{\rho}{(c-a)t} \ln \frac{(c-a)x_2 + (d-b)}{(c-a)x_1 + (d-b)} \\
&= \frac{\rho}{(c-a)t} \ln \frac{(c-a)(x_1+h) + (d-b)}{(c-a)x_1 + (d-b)}
\end{aligned} \tag{3.18}$$

Let $x_1 = 0$, the resistance of the entire trapezoid is:

$$R = \frac{\rho}{(c-a)t} \ln \frac{(c-a)h + (d-b)}{(d-b)} \tag{3.19}$$

Define the length of the two parallel width sides as $L_1 = (d-b)$, and $L_2 = (c-a)h + L_1 = (c-a)h + (d-b)$, where h is the height, the resistance can be simplified as:

$$R = \frac{\rho h}{(L_2 - L_1)t} \ln \frac{L_2}{L_1} \tag{3.20}$$

3.3.1.3 Sensitivity of the trapezoid resistors

The sensitivity can be represented by gauge factor. According to equation (3.20), for isotropic linear elastic materials, we have

$$R = \frac{\rho h}{(L_2 - L_1) \cdot l \cdot t} \ln \frac{L_2 \cdot l}{L_1 \cdot l} \tag{3.21}$$

Where L_1 and L_2 are constants. Rewrite the above equation to

$$R = \frac{\ln(L_2 / L_1) \cdot \rho h}{(L_2 - L_1) \cdot l \cdot t} \tag{3.22}$$

$$\frac{dR}{R} = \left(\frac{d\rho}{\rho} + \frac{dh}{h} - \frac{dt}{t} - \frac{dl}{l} \right) \cdot L \tag{3.23}$$

L is a constant as $L = \frac{\ln(L_2 / L_1)}{(L_2 - L_1)}$.

Consider the uniaxial tension in the x direction, we have

$$\frac{dt}{t} = \frac{dl}{l} = -\nu \frac{dh}{h} \quad (3.24)$$

Where ν is the Poisson's ratio and $\frac{dl}{l} = \varepsilon_{axial}$.

Thus equation (3.23) can be converted to

$$\frac{dR}{R} = \left(\frac{d\rho}{\rho} + (1 + 2\nu) \frac{dl}{l} \right) \cdot L \quad (3.25)$$

According to the definition of the gauge factor as mentioned in 3.2.2, the gauge factor for a trapezoid shape resistor is:

$$\frac{dR/R}{\varepsilon_{axial}} = \left(\frac{d\rho/\rho}{\varepsilon_{axial}} + (1 + 2\nu) \frac{dl}{l} \right) \cdot L \quad (3.26)$$

Compared to equation (3.9), equation (3.26) has an extra term L which is determined by the size of the two parallel size. When changing the magnitude of L, it is possible to increase the sensitivity of the sensor.

3.3.1.4 Ring shape

Since in vessel pressure test, the force is applied perpendicular to the surface of the strain gauge thin film, it is better to have thin film shape with high symmetry. The ring shape is thus employed. When static uniform pressure is normally applied to the surface, the deformation of the ring thin film would be the same in any directions.

3.3.1.5 The resistance of ring resistors

For convenience, the resistance of ring shape resistors are derived in polar coordinate system, as shown in Figure 3.8.

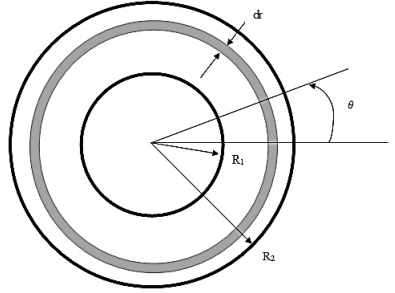


Figure 3.8 Ring and sector shape

The resistance of the full ring will be derived from integration of the resistance of a sector with angle θ

$$dR = \rho \frac{dr}{r \cdot \theta \cdot t} \quad (3.27)$$

Integrate along the r direction and consider dR in serial,

$$R = \frac{\rho}{t \cdot \theta} \int_{R_1}^{R_2} \frac{dr}{r} \quad (3.28)$$

$$R = \frac{\rho}{t \cdot \theta} \ln \frac{R_2}{R_1} \quad (3.29)$$

For the full ring, $\theta = 2\pi$,

$$R = \frac{\rho}{t \cdot 2\pi} \ln \frac{R_2}{R_1} \quad (3.30)$$

Where t is the thickness of the thin film, R_1 and R_2 are the inner and outer radius of the ring, and ρ is the resistivity of the material.

3.3.1.6 Sensitivity of the ring resistors

For isotropic linear elastic material, assume $R_1 = r \cdot r_1$ and $R_2 = r \cdot r_2$, where r is a variable, and r_1 and r_2 are constants. Based on equation (3.30)

$$R = \frac{\rho}{t \cdot \theta} \ln \frac{r_2}{r_1} \quad (3.31)$$

$$\ln R = \ln(r_2 / r_1) \cdot (\ln \rho - \ln t - \ln \theta) \quad (3.32)$$

Take derivative on both sides of equation (3.32)

$$\frac{dR}{R} = \ln(r_2 / r_1) \cdot \left(\frac{d\rho}{\rho} - \frac{dt}{t} - \frac{d\theta}{\theta} \right) \quad (3.33)$$

Since $\frac{dt}{t} = \varepsilon_z$, $\frac{d\theta}{\theta} = \varepsilon_\theta$, and $\frac{dr}{r} = \varepsilon_r$, the equation (3.33) can be rewritten as

$$\frac{dR}{R} = \ln(r_2 / r_1) \cdot \left(\frac{d\rho}{\rho} - \varepsilon_z - \varepsilon_\theta \right) \quad (3.34)$$

From Barlow's Equation, the stress found is σ_r . Although the linearized Hook's Law doesn't apply in this case, it has been proved that the change in resistance and pressure have a linear relationship between them [57]. So a smart way to define the sensitivity of the ring shaped pressure sensor is to directly relate the pressure with the resistance change by

$$Sensitivity = \frac{\Delta R / R}{P} \quad (3.35)$$

In this case, if the ring is placed on the center of the channel, the deformation only varies on radius direction and the deformation on thickness direction $\varepsilon_z = -\nu\varepsilon_r$ and $\sigma_r = E\varepsilon_r$, from equation (3.30)

$$\frac{dR}{R} = \frac{\ln(r_2 / r_1)}{2\pi} \cdot \left(\frac{d\rho}{\rho} + 2\nu\varepsilon_r \right) \quad (3.36)$$

Combine with the definition, the gauge factor defined as following

$$\frac{dR/R}{\varepsilon_r} = \frac{\ln(r_2/r_1)}{2\pi} \cdot \left(\frac{d\rho/\rho}{\varepsilon_r} + 2\nu \right) \quad (3.37)$$

3.3.2 Conclusion and discussions

From previous research done by Qiuyan Li, who has fabricated the CNT-PI nanocomposite strain sensors, the sensitivities of the thin film of rectangle, trapezoidal and ring shape are compared in Figure 3.9 [57]. The difference of the sensitivity of rectangular and trapezoidal thin film can be proved by the definition of the gauge factor, which in this case is $h_2/h_1 = 2$, it is easy to tell that the sensitivity of the trapezoid pattern is smaller than that of the rectangle. Unfortunately, the gauge factor of ring shaped thin film isn't comparable with the other two because the definitions of them are different. But this result could explain the different 'gauge factor' from two different testing method (i.e. tensile testing and pressure vessel).

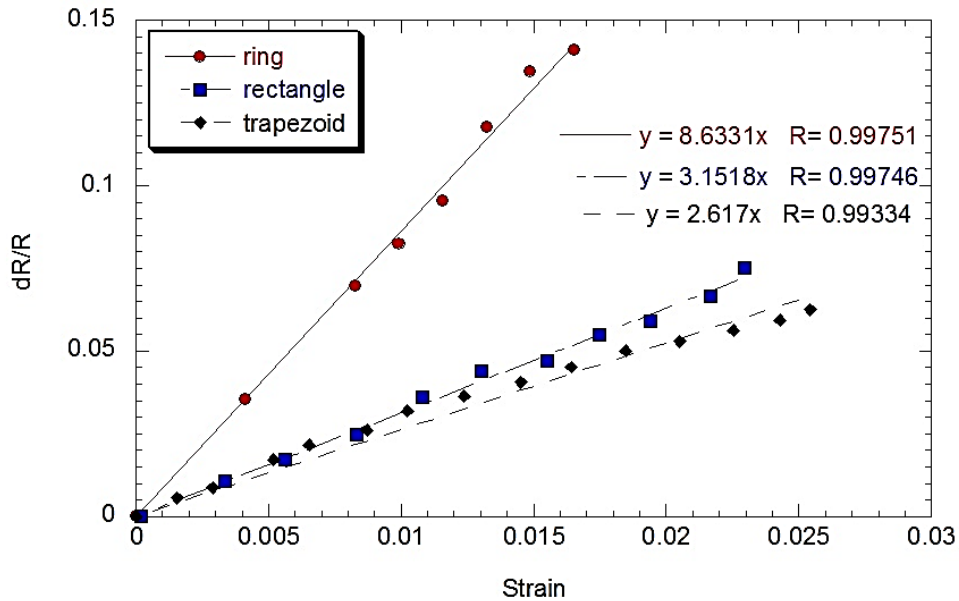


Figure 3.9 Sensitivity comparison of rectangular, trapezoid and ring shape CNT-PI nanocomposite sensors [57]

3.4 GRAPHENE-PI NANOCOMPOSITE FABRICATION

There are two major parts to fabricate the graphene-PI nanocomposite. The first one is to produce the graphene-PI nanocomposite solution with graphene weight ratio gradient, and the second one is to deposit the nanocomposite onto the insulated polyimide thin film. For the first step, the quality of the suspension solution is extremely significant, which mainly affects the mechanical properties, electrical property and piezoresistivity of the graphene-PI nanocomposite. The major reason to affect the quality of the nanocomposite solution is the distribution of graphene in the suspension. If graphene is not dispersed well, graphene will be inhomogeneous in the suspension. Then no matter how uniformly it is deposited on the substrate, the mechanical and electrical properties as well as the piezoresistivity of the nanocomposite film are not consistent. The result from the test will be unreliable and lack of repeatability, making it impossible to calibrate the sensitivity of the nanocomposite strain gauge. Therefore, proper fabricating procedure should be adopted, and graphene has to be distributed homogeneously at each fabricating steps. Only in this way can it be possible that the final graphene-PI nanocomposite suspension have a satisfactory quality. With the high-quality nanocomposite suspension fabricated, the thin film strain gauge shall be made. Because of the small viscosity of the suspension, it can easily move around on the polyimide thin film substrate, and because of the influence of surface tension and coffee-ring effect [59], it is not easy to guarantee the uniformity of the nanocomposite thin film. Upon this, ink-jet printing method is introduced to deposit the nanocomposite suspension. By ink-jet printing method, it is easy to control the amount of the suspension, and it is also possible to precisely control the location of the suspension drops. In this case, the uniformity of the nanocomposite thin film is guaranteed. After heated and well cured, the sample is ready to be tested.

3.4.1 Graphene-PI nanocomposite suspension fabrication

The graphene nanocomposite suspension is fabricated by simple blending method. The graphene solution was dispersed in suitable solvent, and the amount of both graphene solution and polymer needed to obtain different graphene weight ratio was calculated, then the graphene solution was mixed with the polyimide at room temperature, and put the mixture into ultrasonic water bath to make the graphene distributed homogeneously.

Consider good chemical compatibility, dimethylformamide (DMF) is chosen to dilute graphene. The mixture of graphene with DMF is commercially available through Cheap Tubes Inc. and it can serve as graphene source. This solution contains graphene in a ratio of 75mg/100ml, and was put into ultrasonic bath for at least two hours before use to assure fully distribution of the graphene solution. The base fluid polyimide (PI) is PI2611 from HD ® Microsystem (1 Gal, Parlin, NJ, USA). The PI2611 was diluted into n-Methyl-2-pyrrolidone (NMP, from Sigma-Aldrich®, 1L, St. Louis, Mo, USA) with weight ratio of 1:2. The mixture was then stirred by a magnetic bar at a speed of 800rpm at room temperature for two hours to create uniform PI solution. Next, the purchased graphene solution was toned with varying amount of the above PI solution to create the nanocomposite with different graphene weight ratios ranging from 1.0wt% to 1.8wt% with a step size of 0.2wt%. For examples, the mixing ratio of graphene solution to PI solution for 1.0wt% sample is 1000: 236.4, 2wt% sample is 1000:118.1. Before usage, the mixture of the graphene solution and PI solution were brought into ultrasonic water bath and vibrated for 3 hours up to form thoroughly homogenous solutions, and always have the mixture solution ultrasonic bath for 2 hours before usage.

3.4.2 Printing procedure

Ink-jet printing technology is used due to its convenience and repeatability, with this technique, the shape of the thin film can easily be specified, and the size can be tremendously reduced, which gives a lot of advantage to apply on those with complex and tight structures and strain measurement has to be conducted.

The equipment for ink-jet printer is called JetLab, the version of the software program to run the ink-jet printer is JetLab 4. The ink-jet print station is shown in Figure 3.10, the polyimide film was placed at the substrate plate, the x y stages control the movement of the substrate plate in x, y directions, and the z stage moves the print head up and down in z direction, the camera could inspect the drops coming out of the print head, making the drop analysis possible. During printing process, the tip of print head is usually 1.5 mm to 3 mm high to the substrate.

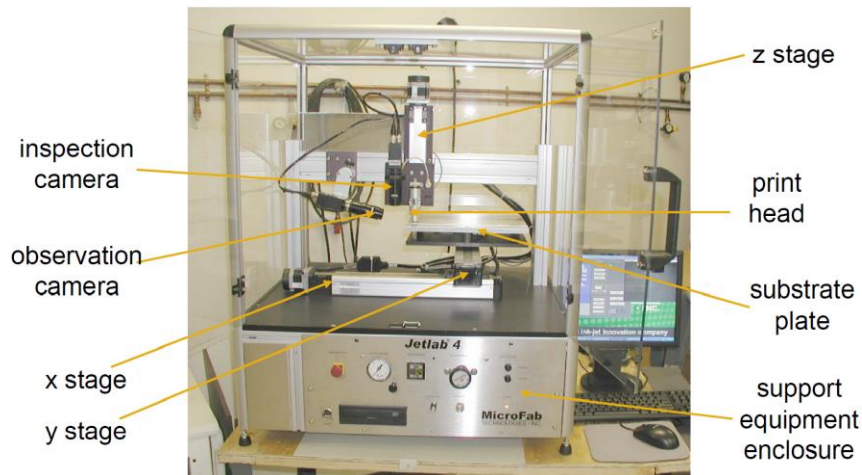


Figure 3.10 Ink-jet print station

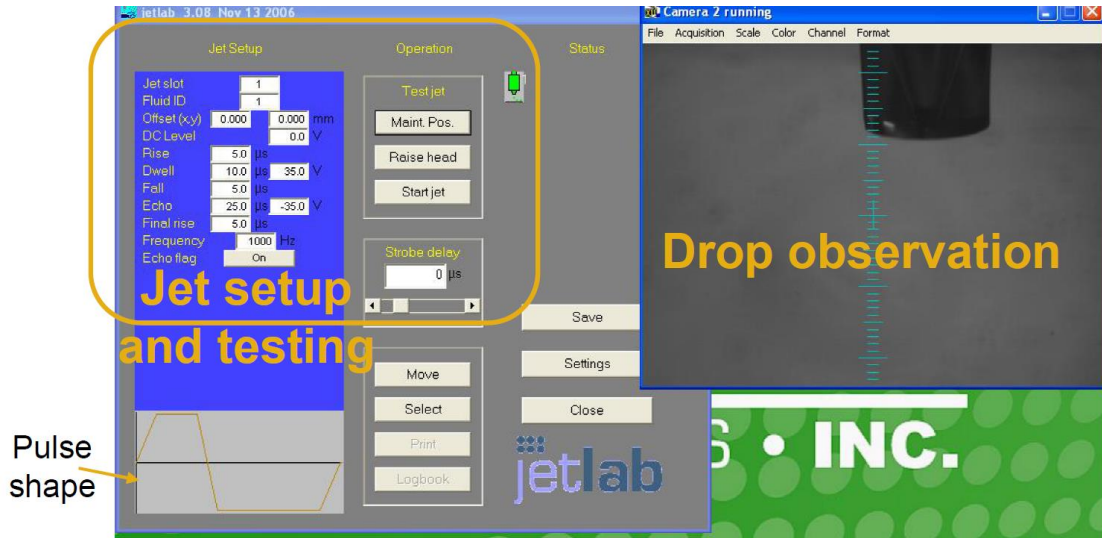


Figure 3.11 Drop monitor on the computer

The drops can be monitored by a program called JetLab 4 on the computer, therefore, drop analysis can be executed. In every run of drop analysis, the camera will capture the real-time drops 3 times in a sequence, and calculate the average velocity, volume, diameter, polar angle and planer angle of the drops. The result of drop analysis is shown in Figure 3.12.

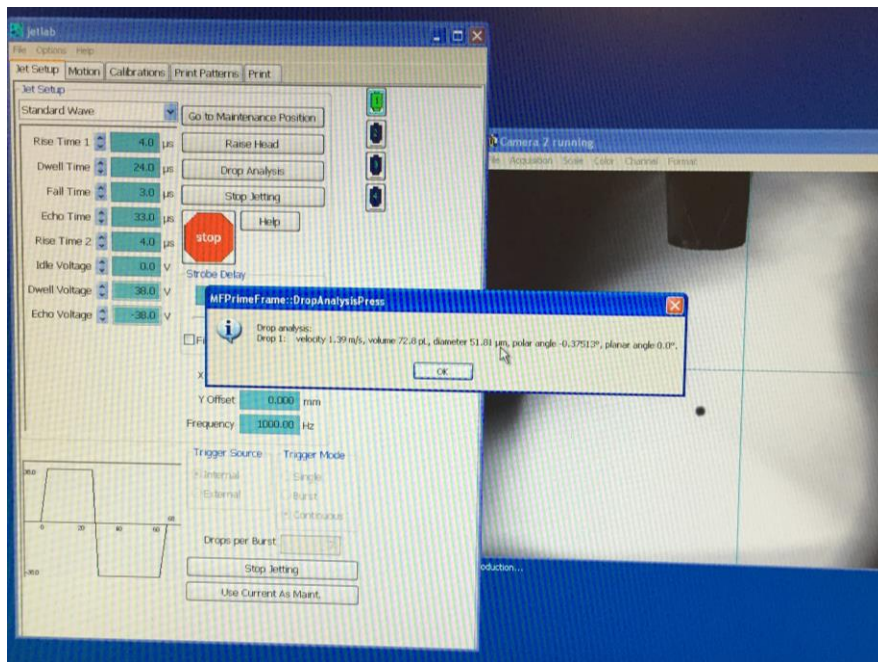


Figure 3.12 Drop analysis results

Ink-jet printing technique consists of two major steps: drop generation and printing pattern design. The drops should be stable and consistent. By stable, the drops should have relatively steady sizes and should have less or better no satellites, satisfactory drops are as shown in Figure 3.13.

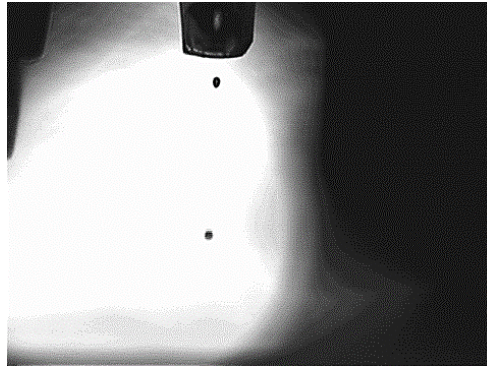


Figure 3.13 Favorable drops formation

Although the ambient air pressure and humidity can play a role to the work of the ink-jet printer, the critical parameters affect the drop formation are the pressure inside the syringe solution reservoir and the wave function (wave form) of the electrical pulse applied to the piezoelectric layers in the print head. The pulse shape to fire the jetting devices (a) and a close view of drop generation procedure (b) are shown in Figure 3.14. To obtain satisfactory drops, the parameters have to be toned by adjusting the amplitude of the dwell and echo dwell voltage, rise time and fall time, and the back pressure added to the syringe reservoir.

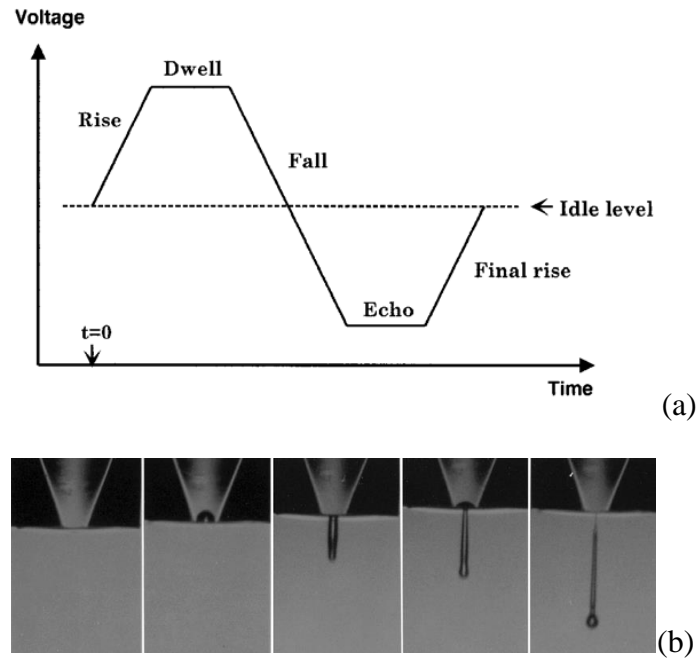


Figure 3.14 (a) Principle of pulse shapes used to fire jetting devices and (b) Close-up view of drop formation [60]

The pulse shape parameters chosen to print graphene-PI nanocomposite on the polyimide substrate are listed in Table 3.1. The magnitude of dwell and echo dwell voltage can fluctuate about 1V around 38.0V, because of the possible humidity and ambient air pressure change.

Table 3.1 Pulse shape parameters

Action	Time (μm)	Magnitude of Voltage (V)
Rise	4.0	----
Dwell	22.0	38.0
Fall	4.0	----
Echo Dwell	33.0	38.0
Final Rise	5.0	----

The back pressure can be adjusted through a rotatory crank in the front of the ink-jet printer box, it usually starts from -2.0kPa, and was adjust around -2.0kPa to -2.6kPa to make sure that the pressure would not be so low that the sample solution could keep leaking out the nozzle no matter how the wave shape parameters were chosen. In the meantime, the back pressure would be large enough to generate drops. Usually the back pressure is around -2.2kPa ~ -2.4kPa (Figure 3.15), again the drop formation can be affected by the ambient atmosphere.



Figure 3.15 Back pressure

Once the wave shape parameters were set, and the back pressure is fixed, the size and the velocity of the drops should be consistent and is barely affected by the concentration of graphene in the nanocomposite solution. This could be explained by that the viscosities of the nanocomposites with different graphene concentration vary so little that have negligible influence on the pulse shape to generate desirable drops.

The nanocomposite solution was printed to a small rectangular shape on bar-shape polyimide substrate for tensile test, while printed to ring shape for pressure test on circular substrate. The printing pattern determines the starting and stopping points of drops, number of drops in x and y directions, step size in each direction and planer angle of the drops, it can be chosen from those already exist in the JetLab program or for other complex patterns, printing recipes can be written down in separate text files by the user and then read and executed by the

JetLab program. The printing pattern of rectangular array is already inserted in the JetLab program, to form a continuous network of nanocomposite material, the drop spacing should be set smaller than the drop size was required so that the adjacent drops would come in contact with each other on the substrate. From drop analysis, the volume of the drop is about 72 pL, and its diameter is about 52 μm , so the 0.05mm (50 μm) step is chosen, the number of drops in x and y directions are 140 and 30 respectively. The full rectangular array pattern in this research is shown in Figure 3.16 (a), and the printing procedure is shown in Figure 3.16 (b). To print ring, the print script was written to create a continuous ring shape network of the nanocomposite, and the inner diameter of the ring is 4 mm and the outer diameter is 5 mm. Three layers of the nanocomposite were printed on both bar and circular substrate and five samples of each shape and each weight concentration were created. In case that drops are missing at some points, multiple layers are demanded, because the later layer will always cover the previous one so the probability of discontinuity could be eliminated. Three layers were chosen for each sample to have enough material on the substrate that electric property (piezoresistivity in this case) can be evaluated by the testing methods. During the printing process, a hotplate of 120 Celsius degrees is used underneath the polyimide substrate so that the previous layer of the nanocomposite solution dried when printing of the following layer started to build. By doing so, the flowing around of the nanocomposite solution on the substrate can be prevented, and the coffee ring effect could be reduced, even if it happened at each individual point, after overlapping by the nearby points and multiple layers covering, it could be finally uniform over the entire nanocomposite film.

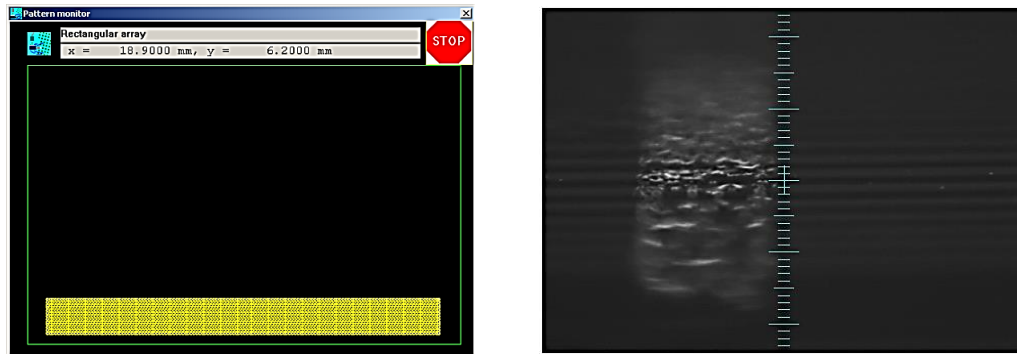


Figure 3.16 (a) Rectangular printing pattern and (b) Printing procedure

3.4.3 Strain gauge fabrication

Having the graphene-PI nanocomposite suspension completed, it can be used to fabricate strain gauge by deposit the solution onto a nonconductive substrate. To accomplish favorable deposition, ink-jet printing method is implemented. Since the nanocomposite solution is dilute, its viscosity greatly decreases, thus the printing method is feasible. In this way, not only the uniformity can be achieved, but also the shape and the thickness of the nanocomposite can be better controlled. Detail printing procedure will be elaborate in the next section.

In order to print the nanocomposites a substrate needed is the one that would not alter the properties of the nanocomposite and not affect the performance of the nanocomposite during strain and resistance testing. Since the nanocomposite was a mixture of PI2611 and graphene, a suitable PI substrate was used to print on. Therefore, the Kapton® Polyimide thin film with thickness of 5 mil (127 μ m), purchased from Dupont Company, is used as the substrate on which the graphene-PI nanocomposite was deposited. The polyimide film was cut into rectangular and circular pieces for tensile test and pressure test respectively, and the nanocomposite will be deposit on the center of those substrate pieces. After deposition, the sample was heated at 120 Celsius degrees on a hot plate for about 3 minutes to fully dry the nanocomposite on the

substrate. Later on, the nanocomposite film elements on PI substrate were fully cured at 270°C for 90 minutes in the oven.

To connect the graphene-PI nanocomposite thin film elements to the measurement system, interdigitated transducer (IDT) electrodes and concentric circle electrodes are coated on the substrate by sputter coater and shadow mask. The sputter coater is from (company). An Argon gas tank was connected to the chamber of the sputter coater, along with a gas flow regulator, and the gas flow was adjust to about 6 psi before turning on the sputter coater. Sputter coat is a sputter deposition process to cover a specimen with thin layer of conductive metal. As shown in Figure 3.17, the specimen is put on the substrate, the chamber is pumped vacuum until the pressure is less than 0.04 mbar and an electrical and magnetic field is added between the target and the substrate, the argon ion would hit the target wafer and eject the metallic atoms out of the wafer, accelerate by the electric field, the gold atoms hit on the surface of the specimen. In this research, a gold circular wafer is used as a target, and the specimen was coated for 90 minutes.

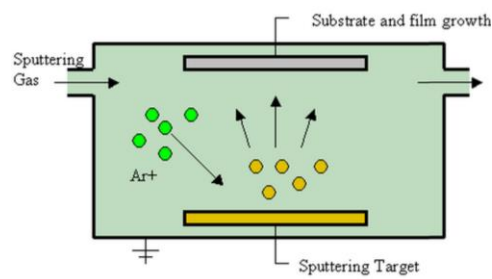


Figure 3.17 Sputter coating mechanism

Before coating, shadow masks are fabricated to shape the electrodes into interdigitated and concentric circles. The masks are created by 3-D printing technology. The masks should not be too thick, otherwise, the gold atoms will have difficulty arriving at the polyimide film, which

probably causes non-conduction of the electrodes since the gold layer could be too thin. In this thesis, the thickness of the mask is 0.8 mm. The masks for coating interdigitated and concentric circular electrodes are shown in Figure 3.18. The polyimide film with graphene-PI nanocomposite deposited on will be fixed on a silicon substrate, and the mask will be fixed on the upper surface of the polyimide film, leaving the nanocomposite in the middle, then specimen for coating is ready, as shown in Figure 3.19.

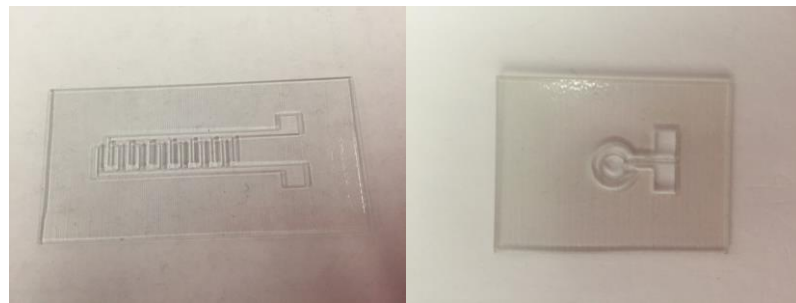


Figure 3.18 Masks for interdigitated and concentric circular electrodes



Figure 3.19 The specimen ready for coating

The spin coating was conducted by Cressington 108 Sputter Coaters, as shown in Figure 3.20, the specimen ready for coating is placed on the substrate inside the chamber. The coating

process starts with placing the cap well and open the gas valve, then the power can be opened. The pump system will pump the pressure in the chamber down to 0.04 mb, then coating for 90 seconds. Then the electrodes are coated on the substrate.

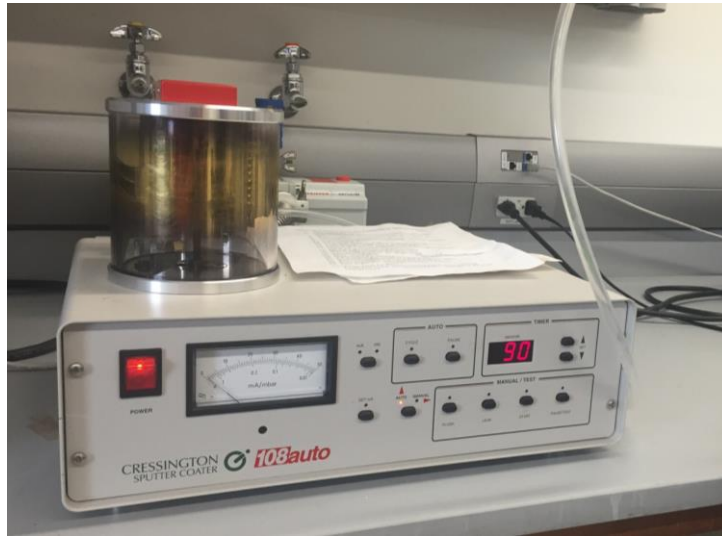


Figure 3.20 Cressington sputter coater

Copper wires with insulant coat were used to connect the electrodes to the measure equipment. Since the copper wires are very thin, with a diameter about 0.2 mm, to guarantee well connection, the connection areas were enlarged by wiping off the insulant coat on both ends of the copper wires and pasting small rectangular aluminum foil paper onto the nude ends of the copper wires, on the end to connect to the measurement equipment, the copper wire was even wrapped in the aluminum foil paper. Silver paste was also applied to act as a bonding to glue the nude copper wire ends to the electrodes or the foil paper, for it has high conductivity when dried, thus can make the connection stay strong.

4.0 PIEZORESISTIVE PROPERTY CHARACTERIZATION OF GRAPHENE-POLYIMIDE NANOCOMPOSITE

4.1 GRAPHENE-PI NANOCOMPOSITE RESPOND TO UNIAXIAL LOAD

One of the most common and simple way to determine the gauge factor of a device and to study its piezoresistive property is to conduct the uniaxial tensile test, and keep track of its resistance change when applying load. To achieve this goal, graphene nanocomposite suspension will be precipitated on a rectangular polyimide tensile test substrate, and will be well cured and firmly attached to the substrate. Therefore, the deformation of the nanocomposite thin film and the substrate is coinstantaneous, and the difference is so small that could be neglected so that we can assume that the load as well as the longitudinal strain on the graphene nanocomposite thin film are equal to that of the polyimide substrate. Thus, by measuring the longitudinal strain on the substrate and simultaneously recording the corresponding resistance, the gauge factor of the nanocomposite with various graphene concentration could be further calculated.

4.1.1 Experiment Setup

With ink-jet printing method, the graphene nanocomposite was homogeneously deposited on the polyimide substrate. The substrate were 105mm by 15mm rectangular pieces, and the nanocomposite was deposited in the center of the substrate with the dimension of a 7mm by

1.5mm rectangle, as shown in Figure 4.1. After 3 hours in oven, the nanocomposite was fully cured and stiffly stock on the substrate. In this case, we can assume that the deformation of the graphene nanocomposite thin film is the same as the deformation of the substrate, so as the longitudinal strain on the nanocomposite film and that on the substrate. In order to measure the corresponding resistance when the sample suffers strain, interdigital transducer is coated on the substrate as electrode. The nanocomposite thin film is made lying in the center.



Figure 4.1 Rectangular nanocomposite thin film



(a) AP8214 from Pasco



(b) current/voltage source measure unit



(c) GBIP controller

Figure 4.2 Uniaxial testing equipment

The equipment used to apply uniaxial load is a stress/strain apparatus, as shown in Figure 4.2 (a) (AP8214 from Pasco), which is equipped with a force sensor to calculate stress automatically and a rotary sensor to measure displacement/strain. The uniaxial force load can be added through a rotatable crank. Underneath the apparatus is what is called the ScienceWorkshop® 750 which can collect the data every 0.1 second and can input real time data

into a computer with a software DataStudio to record the data. Meanwhile, through the two sides of the electrodes, the nanocomposite thin film is connected to a current/voltage source unit (Figure 4.2 (b), Keithley 238), in which a Wheatstone bridge was built and a 10 volts DC voltage can be provided constantly. With the current and voltage information, the real time resistance can thus be achieved through a Labview program, which record the data every 1 second. To transfer the real time data into LabView, a GPIB controller (by National Instrument) is introduced, as shown in Figure 4.2 (c).

During the test, the polyimide thin film substrate is mounted on the stress/strain apparatus with two ends fixed tightly, before the test starts, the film is relax with zero external force. At the left end, there is a cantilever beam associate with the tensile sample, when the sample is straight and ready to suffer stress, the tip of the cantilever beam will contact with the force sensor, and the data will start to be collected by DataStudio. By slowly and evenly rotating the crank clockwise, a uniaxial load is applied on the substrate. In the meantime, the real time resistance of the nanocomposite is read by LabView program.

4.1.2 Result and Discussions

By testing on the samples of 5 different graphene concentrations, i.e. from 1.0wt% to 1.8% with a step size of 0.2wt%, the normalized resistance change $\frac{dR}{R}$ vs the longitudinal strain ε (caused by uniaxial force in the same direction) can be plotted, as shown in Figure 4.3. It suggests that for each graphene concentration, the resistance of the graphene-PI nanocomposite increase as the external extensional load is applied. This phenomenon can be explained by the tunneling effect on semiconductors as demonstrated in Chapter 3, under extension, the distance between adjacent

graphene sheets increases, making electrons transportation through tunneling more difficult, which is reflected as overall increase in resistance.

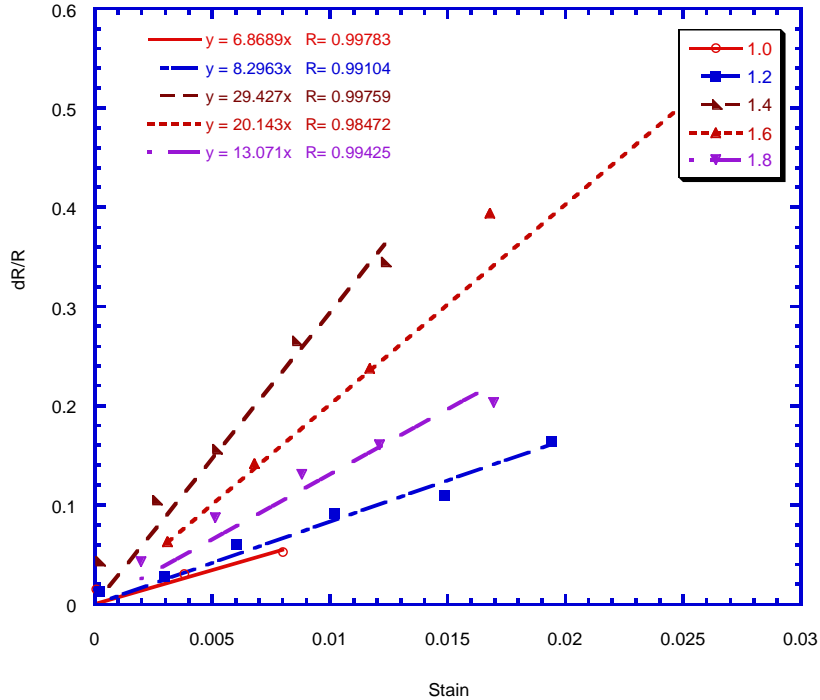


Figure 4.3 Normalized resistance change vs strain in different graphene concentration

The normalized resistance change and the strain change exhibit approximately linear relationship, and the slope of the trend line is the gauge factor, as defined in equation (3.10). And the gauge factors of different graphene concentration are summarized and compared in Figure 4.2. The percolation threshold theory suggests that the threshold for graphene-PI nanocomposites is between 0.8wt% to 1.8wt%, and from 0.8wt%, as the graphene concentration increases, the gauge factor increases at first, then decreases. The largest gauge factor occurs at 1.4wt%, so it is the optimum graphene concentration for strain sensing, and the largest gauge factor is 26.57.

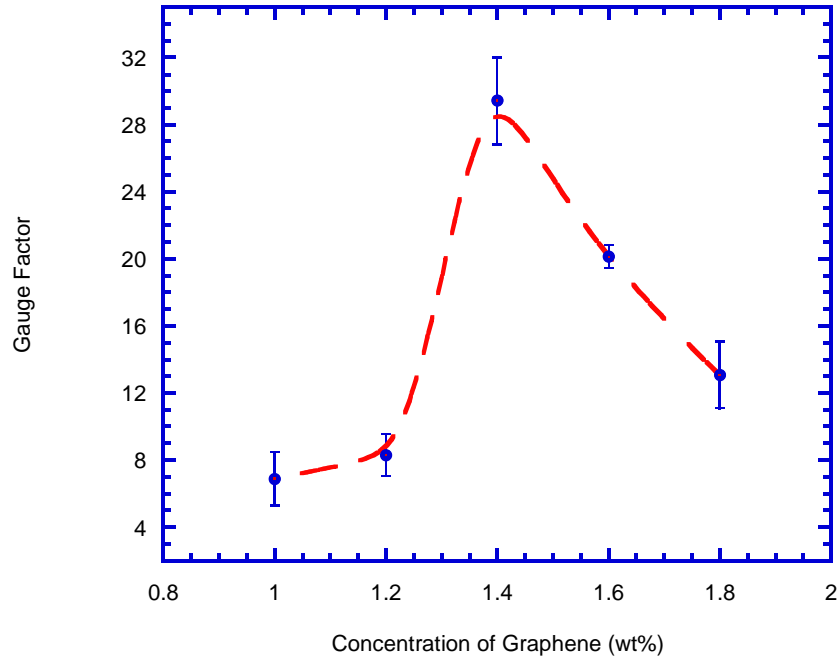


Figure 4.4 Gauge factor at each concentration

Also the deviation of every gauge factor is analyzed in Table 4.1, from which, the maximum deviation of each gauge factor is less than 2, and the standard deviations are very small, indicating that the real gauge factor only fluctuate a little from the average value, the data to describe piezoresistive property of graphene-PI nanocomposites is reliable, thus we can use the average gauge factor to represent the gauge factor of the nanocomposite thin film with certain graphene weight ratio.

Table 4.1 Table summary and error analysis of gauge factor

Graphene concentration (wt%)	1.0	1.2	1.4	1.6	1.8
Average gauge factor	6.87	8.30	29.43	20.14	13.07
Maximum deviation	(+)1.58	(+)1.24	(+)2.58	(+)0.69	(-)1.97
Standard deviation	0.877	0.894	0.246	0.457	0.711

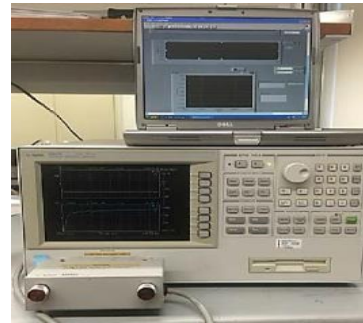
4.2 GRAPHENE-POLYIMIDE NANOCOMPOSITE RESPOND TO PRESSURE

To explore the respond of graphene nanocomposites to pressure, a series of experiments were conducted. These pressure tests can also be used to determine the gauge factor of graphene nanocomposite with different weight ratio. Pressure tests were conducted using a pressure vessel (shock tube), a certain quantity of gas flow was used to generate a certain intensity of pressure, and the piezoresistive property of graphene nanocomposite was studied by analyzing its resistance change. An electrical impedance analyzer was implemented to collect and record the impedance of a sample.

The graphene nanocomposite was fabricated on the center of circular polyimide substrate, the diameter of the substrate is about 90mm, which is a little larger than the inner diameter of the pressure vessel, in this case, the sample could be completely sealed in the vessel, and the pressure could be uniformly added on the surface of the circular sample. The effective part of the sample is a concentric circular ring of graphene-PI nanocomposite, the out diameter of the outer circle is 5mm, and the inner diameter is 4mm. The graphene suspension was deposited on a thin polyimide film by ink-jet printing method, which allows to fabricate tiny devices with exact desired shapes and sizes. The concentric circular electrodes were coated on the substrate, sharing the same center with the nanocomposite thin film, and sandwiched it in the between. A pair of copper wires with insulation coat were used to connect the electrodes with the electric impedance analyzer, and the insulation coat on both ends of the wires were rubbed off to ensure high-quality connection. By testing the impedance of the samples, the practicability and repeatability would be examined.

4.2.1 Experiment Setup

The equipment for pressure testing is showing in Figure 4.5, including (a) a pressure vessel with pressure meter, (b) external gas supply with adjustable pressure regulator, (c) an electric impedance analyzer (Agilent 4294A), a laptop with a LabView program to record the impedance. During the test, the graphene nanocomposite sample was sealed in the pressure vessel, and gas flow continuously hit on the back of the polyimide film, hence the thin film was under extension. At each different intensity of pressure, the deformation of the sample was stationary, which resulted in stationary strain, so it is possible to precisely identify the resolution for the nanocomposite working as strain/pressure sensor. Consequently, this graphene nanocomposite can be manufactured as sensitive pressure sensor after calibrating the gauge factor.



(a) Pressure vessel with meter (b) Gas support with adjustable pressure regulator (c) electric impedance analyzer

Figure 4.5 Pressure test equipment



Figure 4.6 Vessel for pressure test

The pressure vessel is consist of two tubes, in this thesis, they will be mentioned as left part and right part. The sample was fixed on the left part facing the tube, as shown in Figure 4.6. After jointing the two left and right parts together, the sample would be sealed in the vessel. Through the right part, the pressure vessel was also connected to a pressure meter which could monitor pressure intensity, and a compressed gas tank which could provide continuous constant gas flow. In the test, the pressure was risen every 2.5 psi from 5 psi to 15 psi, and the impedance of the nanocomposite was recorded by electric impedance analyzer Agilent 4294A under each pressure intensity. Excited by a small AC current signal, the electric impedance spectroscopy can measure the impedance of a device by measuring the voltage drop across the device over a frequencies range, and that will produce the frequency spectra of resistive and reactive components of the equivalent electrical impedance of the device. Based on these data, a Cole-Cole plot can be plotted. In this research, the sweeping frequency range from 40Hz to 110Hz, and can produce a complete semi-circle Cole-Cole plot.

4.2.2 Results and discussions

The responds of the graphene-PI nanocomposites with different graphene concentration to pressure are show in Figure 4.7 to Figure 4.11 (cole-cole plot for each concentration), which indicate how impedance changes with the pressure variation.

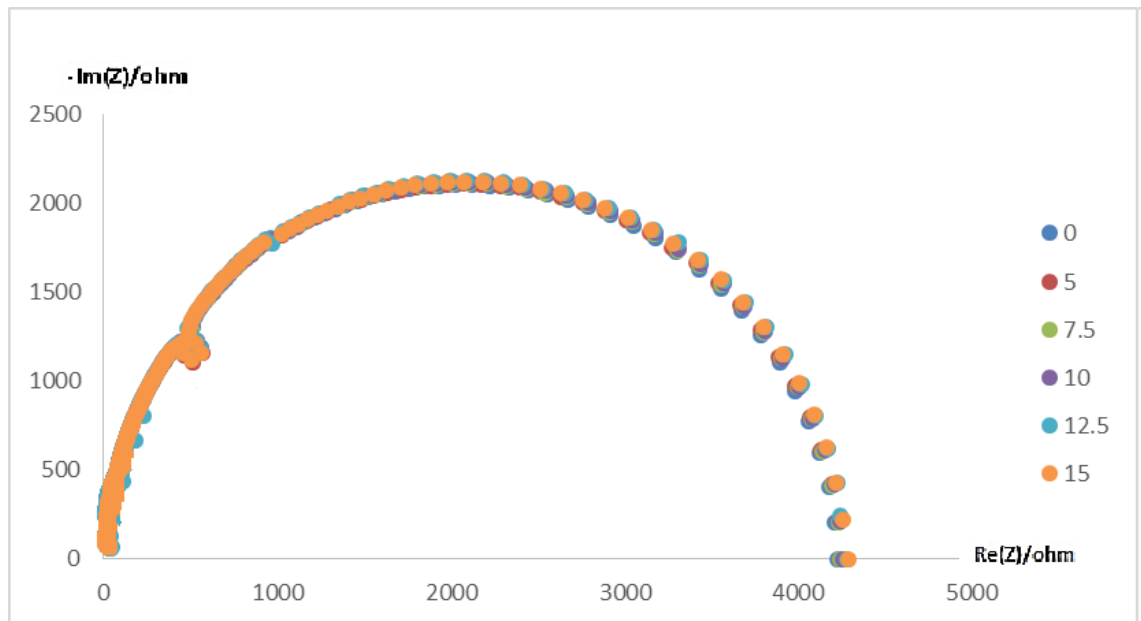


Figure 4.7 Impedance of test sample with CNT concentration of 1.0wt%

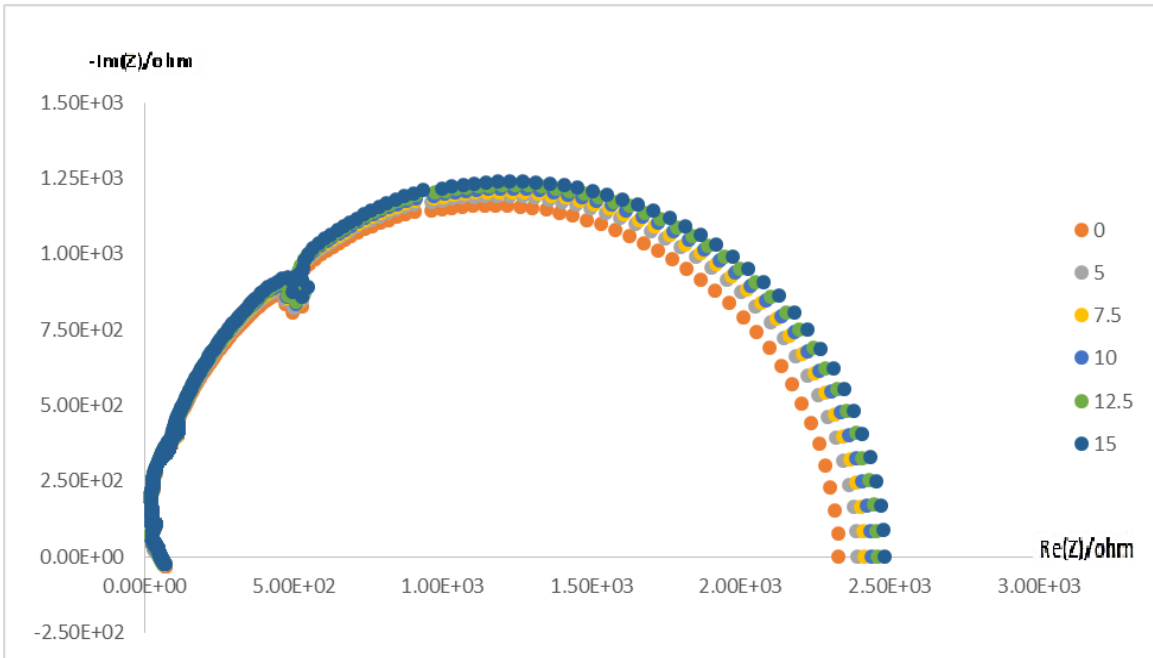


Figure 4.8 Impedance of test sample with CNT concentration of 1.2wt%

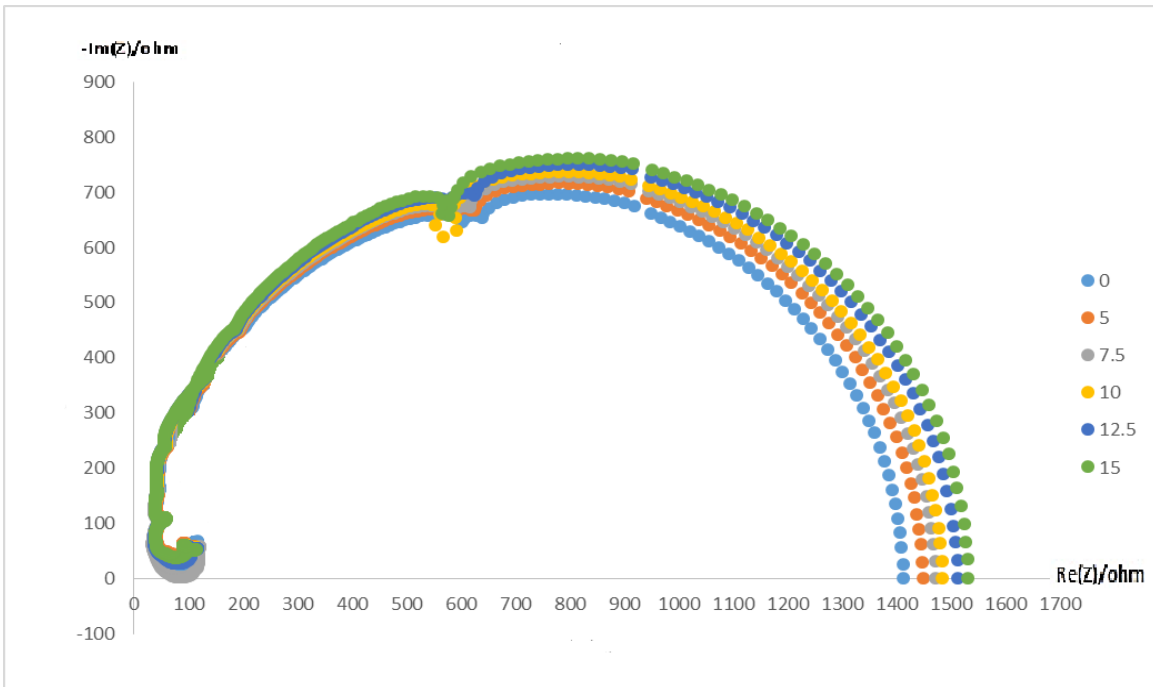


Figure 4.9 Impedance of test sample with CNT concentration of 1.4wt%

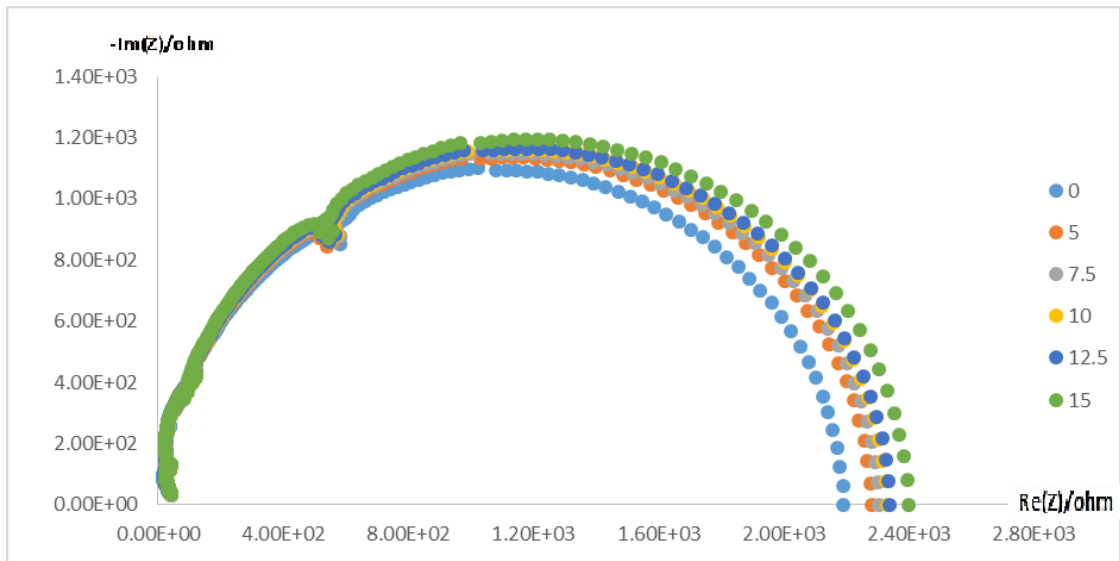


Figure 4.10 Impedance of test sample with CNT concentration of 1.6wt%

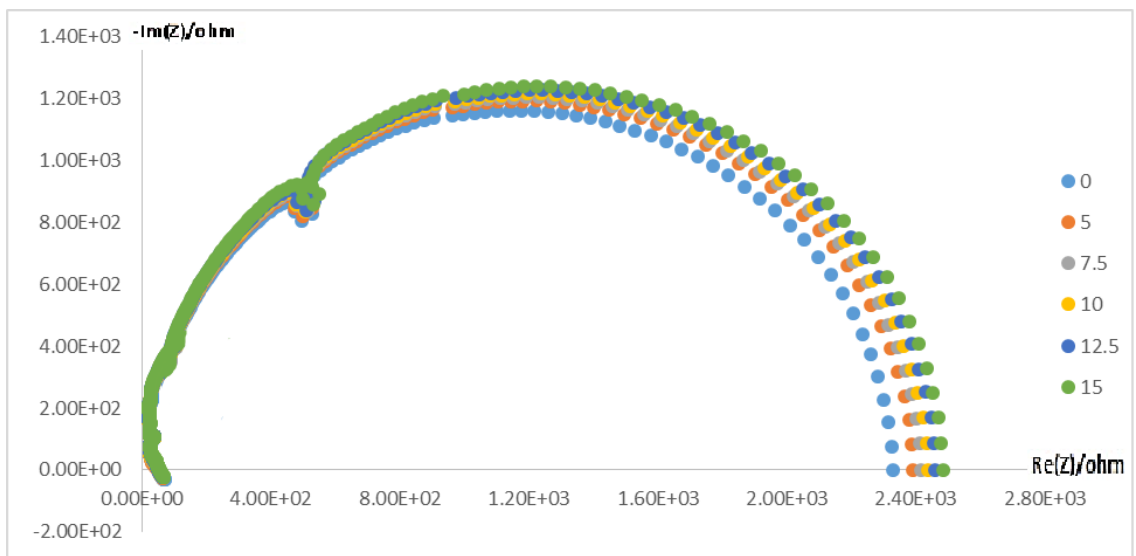


Figure 4.11 Impedance of test sample with CNT concentration of 1.8wt%

Based on Barlow's formula, the stress on the substrate can be calculated from the applied pressure and the geometric dimension of the substrate. Combined with the linearized Hook's

law, the strain can be further calculated. Since the von de Waal's force is very strong between the nanocomposite thin film and the substrates, so it is assumed that the strain of the nanocomposite thin film is equal to that of the substrate, the relationship of impedance and the strain can be estimated and gauge factor can be further calculated.

Table 4.2 Strain generated by pressure

P (psi)	Stress (psi)	Strain
0	0	0
5	1500	0.004137
7.5	2250	0.006205
10	3000	0.008274
12.5	3750	0.010342
15	4500	0.012410

The strain corresponds to different intensity of pressure is list above in Table 4.2.

The relationship between resistance change and strain can be plotted and the gauge factor can be calculated by the slope of the linear trend line, as show in Figure 4.12, the normalized resistance change is positively proportional to the strain.

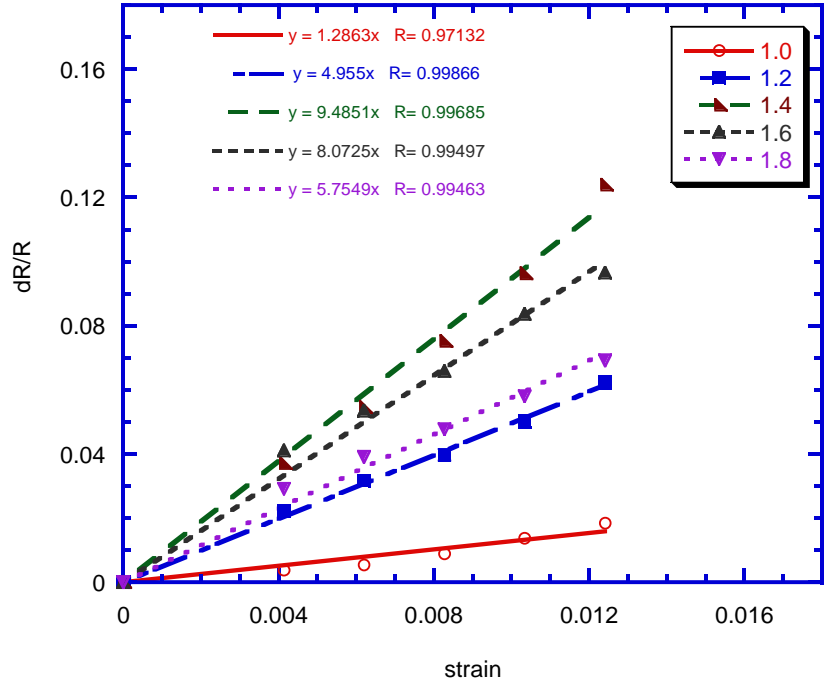


Figure 4.12 Resistance change with strain and gauge factor

The gauge factors with each concentration are summarized in Table 4.3 and Figure 4.13, from which one can see that the gauge factor first rises then comes down as the graphene concentration increases. The largest gauge factor comes out at 1.4wt%, which is about 9.4851. The gauge factor calculated based on pressure tests is relatively smaller than that from the tensile tests, but the overall changing trend is the same, both have the largest gauge factor at 1.4wt% graphene concentration.

Table 4.3 Gauge factor with different graphene concentration

Graphene concentration (wt%)	1.0	1.2	1.4	1.6	1.8
Gauge factor	1.2863	4.9550	9.4851	8.0725	5.7549

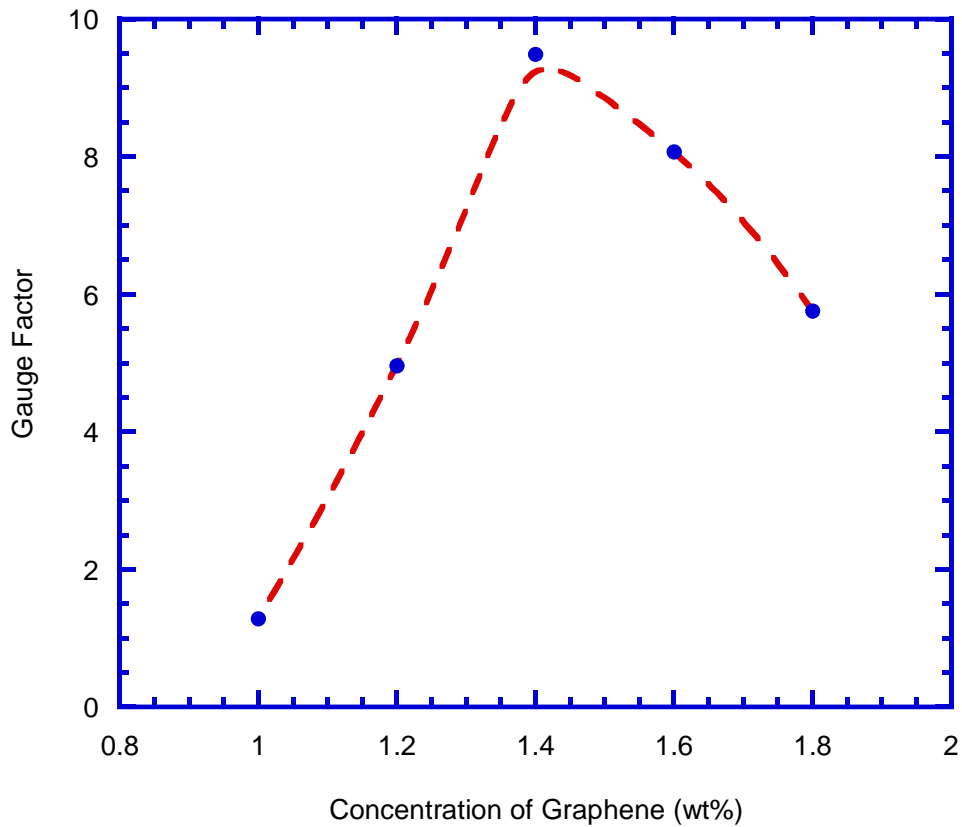


Figure 4.13 Gauge factor with different graphene concentration

4.3 CONCLUSION

4.3.1 Printing technique

The samples created by inkjet printing technique show that the geometry and the size are precisely controlled, and in both tensile tests and pressure tests, those samples performed very well, verifying that using inkjet printing technique to fabricate the nanocomposite thin film strain sensors is a feasible way. Not only feasible, it can be a preferred methods because it gives a way

to design the shape of the thin film. Although the drops deposit on the substrate can cause non-uniform at each drop, but it is compensated by make the drops contacted and even overlap at the edges, so the nanocomposite thin film can be overall uniform. This method can also reduce the coffee ring effect in the overall thin film, and hotplate is also implemented to dry the nanocomposite suspension, and the previous layer is almost dried when the next layer starts, in this way, the density of the solution in one layer is not affected by other layers, thus the thin film can be considered as uniform.

4.3.2 Piezoresistivity characterized by tensile test and pressure test

Comparing the results from tensile test and the pressure test, the changes of gauge factor with respect to strain share very similar trend, which is increase at first as the strain increases then decrease as the strain keeps increase, and for both test, the largest gauge factor occurs at graphene concentration of 1.4wt%. However, the magnitude of gauge factor obtained from the two tests are obviously different. The gauge factor from tensile test is larger than that from pressure test. This can be explained by different testing conditions as elaborated below.

There are some factors that may affect the credibility of the results from the tensile test. First of all, during the tensile test the sample is assumed to be under uniaxial load, but absolute uniaxial force is not possible to get. So there is always some deviation of the load direction, and there can be some slight torsion of the substrate when the sample is fixed on the experiment instrument. Therefore, the deformation of the substrate is not the same as the deformation caused by pure uniaxial tension. Another reason is the experiment limitation caused by different programs that are used to collect and record the resistance and the strain. Although those two data is collected simultaneously, the resistance is collected every one second, while the strain is

obtained every 0.1 second. Since the data is recorded in different programs, they have to be matched manually, this could cause misalignment. Besides, the two ends of the electrodes are connected to copper wires by silver paste, adding thickness to the polyimide substrate, when the substrate is under load, the deformation of the substrate may not remain the same along the tension direction.

As for the pressure test, the deformation under certain strain could be the same for every sample, so the impedance can be collected at a relatively steady state, the results also show that the gauge factor from the pressure test is more stable and fluctuates less than that from tensile test. In pressure test, the edge of the sample is fixed and the pressure only applied perpendicular to the sample substrate, the deformation of the sample is almost as expected, the sample is of less freedom of movement, so the experiment condition is better than tensile test. However, there is still errors in pressure test, the deformation of the inner edge of the thin film ring may be different from that on the outer diameter edge, therefore, the gauge factor definition based on uniaxial deformation may not precisely describe the stress strain relationship for the ring shape sample.

5.0 NANOCOMPOSITE RESPOND TO TEMPERATURE

5.1 INTRODUCTION

Temperature variation can cause the change of geometric size of the strain gauge, which gives rise to the resistance change. Since the strain information is measured through the resistance change of the strain gauge, the effect of the temperature must be compensated to minimize the error. In this case, it is necessary to explore the relationship between the graphene-PI nanocomposite resistance variation with temperature fluctuation, and temperature effect on the gauge factor will be discussed.

In this chapter, the theoretical relationship between the temperature and resistance will be first reviewed, then the experiments to investigate this relationship will be designed and the coefficient factor in terms of temperature will be decided. A compensation method will be finally discussed.

5.2 TEMPERATURE COEFFICIENT FACTOR

The conductivities of materials are often affected by temperature, and it is proven that piezoresistive materials are even more sensitive to temperature variation in the ambient

environment than metallic materials do. In hypothesis, the conductivity would not change, the general relationship between resistance and temperature can be approached by

$$R = R_0[1 + \alpha(T - T_0)] \quad (5.1)$$

Where T_0 is the reference temperature, R_0 is reference resistance at reference temperature, and α is the temperature coefficient of the material that is to be determined through experiments.

5.3 EXPERIMENTAL STUDY

5.3.1 Experiment setup and procedure

The testing sample was fabricated the same as the samples for tensile test, the graphene-PI nanocomposites with different graphene concentration were ink-jet printed on rectangular polyimide substrates after ultrasonic water bath, then the samples were heated on hotplate at 120 Celsius degrees and fully cured in the oven at 270°C . Two samples were fabricated at each graphene concentration, three layers were printed on each substrate. Gold electrodes were sputter coated. The strain gauge was fabricated through the same process as elaborated in Chapter 3.

For temperature coefficient determination experiment, two samples are used at each graphene concentration. Hotplate were used to provide a variety of external temperature for the strain gauge. The strain gauges with different graphene concentration were placed on the hotplate, as shown in Figure 5.1. Since the polyimide substrates are very thin, it is assumed that the temperature that the strain gauge suffered is equal to the temperature of the hotplate. Starting from room temperature 20°C in the lab, the temperature was risen to 50°C and was then risen

every 25 °C until 150 °C . Meanwhile, the resistance output of the two electrode ends were recorded under each temperature. Multi-meter was used to measure the resistance.

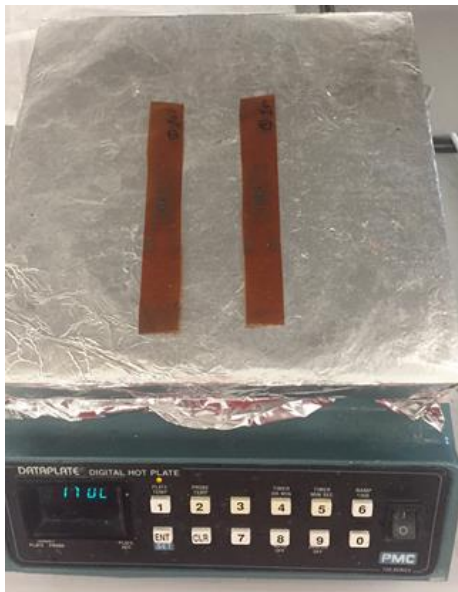


Figure 5.1 Samples placed on hotplate

5.3.2 Experiment results

The resistant impedance change of the nanocomposite samples with graphene weight ratio varies from 1.0% to 1.8% were recorded at each temperature, and the results are discussed later in this chapter.

The graphene-PI nanocomposites are very sensitive to temperature, their resistances change immediately when the actual temperature on the hotplate approaches the targeting value, and in 1 second, the resistance would be steady and remains unchanged until the temperature change again. In general, the resistance decrease as the temperature rise up. Also, as long as the temperature changes between 20 and 150, the thermo-expansion of the transducer remains elastic

deformation, meaning that the resistance will always change back to the original value once the temperature drops back.

5.3.3 Conclusion and discussions

From the definition of temperature coefficient in equation (4.1), it can be calculated by

$$\alpha = \frac{(R - R_0) / R_0}{(T - T_0)} = \frac{\Delta R / R_0}{(T - T_0)} \quad (5.2)$$

The temperature coefficient can be represented by the slope in Figure 5.2, from which one can tell that the resistances of the graphene-PI nanocomposites decrease as the temperature increase, and they have negative linear relationship, so the temperature coefficient should be negative. In the testing procedure, the resistance drops down significantly as temperature rises up, which verifies that it is necessary to work on the temperature compensation, otherwise, if the temperature of the working environment is higher than the temperature in the calibration environment, the resistance change with strain would be under-estimated, and if working environment has the lower temperature, it would be overestimated. Either way will cause an unnecessary error of the strain or pressure measured by this transducers, attenuating the accuracy.

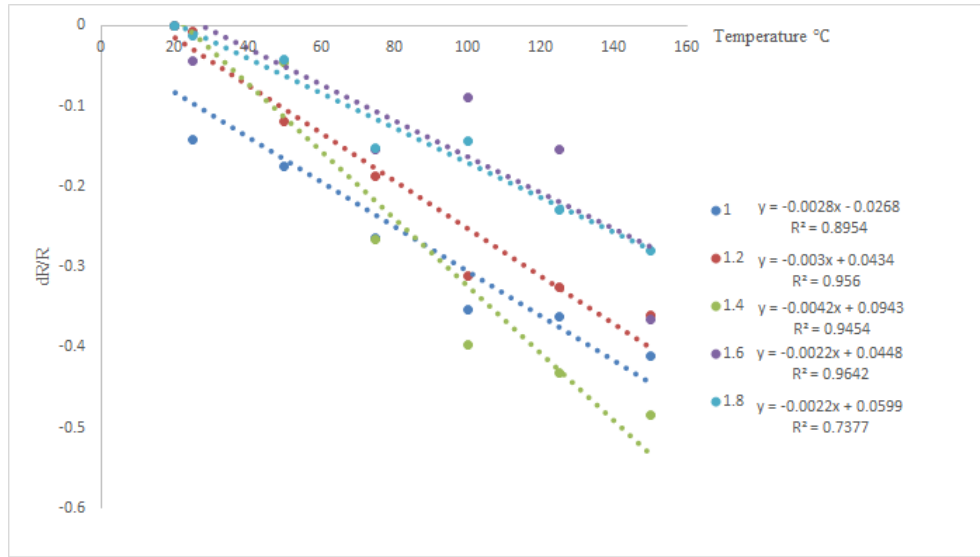


Figure 5.2 Resistance change with respect to temperature

The temperature compensation is a must in semiconductor piezoresistive transducers and sensors. There are several ways to achieve this. One of the simplest ways is to introduce temperature coefficient. The temperature coefficient has been derived and summarized from Figure 5.2, the temperature coefficients are about the same order for all the graphene concentration, the exact value for normalized temperature coefficients at each graphene concentration are listed in Table 5.1.

Table 5.1 Normalized temperature coefficient at each graphene concentration

Graphene concentration (wt%)	Reference resistance (ohm)	Normalized temperature coefficient
1.0	15500	-0.0028
1.2	1189	-0.0030
1.4	747	-0.0042
1.6	1087	-0.0022
1.8	1000	-0.0022

With the temperature coefficient, a dummy gauge can be used or a circuit can be added in the testing Wheatstone bridge to compensate the temperature effect. For a dummy gauge, two identical strain gauges would be placed in two nearby bridges of the whole Wheatstone bridge circuit, like a half-bridge. Both gauges are bonded to the same test specimen, but only one is placed in a position and orientation so as to be exposed to physical strain (the active gauge). The other gauge is isolated from all mechanical stress, and acts merely as a temperature compensation device (the "dummy" gauge). If the temperature changes, both gauge resistances will change by the same percentage, and the bridge's state of balance will remain unaffected. So the difference of resistance between the two strain gauges is only produced by physical force on the test specimen, and the resistance change caused by temperature cannot alter the balance of the bridge.

6.0 CONCLUSION

6.1 PRINTING ADVANTAGES

Previous researchers have utilized spin coating [10], chemical vapor deposit (CVD) [61] and manually painting with brush or chemical droppers [2] to fabricate the nanocomposite thin film on the polyimide substrate. Compared to these traditional methods, inkjet printing method is superior with a lot of advantages.

By inkjet printing method, the geometry of the thin film can be freely designed, and the shape and the size of the thin film can be precisely controlled, the thin film can be printed to any shape in need, by modifying the printing script in JetLab program. Even though there might be some satellites coming out of the nozzle sometimes, causing a slight distortion of the thin film, the deviation is so small that can be neglected. Also, the deviation it can be restricted and eliminate by patiently adjusting the printing parameters. The resolution can be high, based on the lab condition, the size of the nozzle of printer head can be 60 μm or 80 μm which makes drop size around 80 μm or 100 μm respectively. Meanwhile, the location of the suspension to deposit on the substrate can be decided as needed. Not only precise in shape, the size of the thin film created by inkjet printing can be very tiny and it is possible to print on flexible substrate, which is difficult to achieve with spin coating or manually painting. It can be worse for manually

painting, the drop size is so large that it is easy to flow around before the solvent evaporates, and that often cause non-uniform distribution of the material on the substrate.

Although CVD method may control the shape and size of the sample, it often takes a long and complex procedure, and assistant materials are required. The inkjet printing technique provides a time-saving method, the fabricating time can even be further reduced by using multiple printheads, and the fly mode can be applied under certain circumstances. Inkjet printing technique can also greatly reduce the waste at the same time, which almost leaves none material waste. Also, with hotplate, the uniformity of the overall nanocomposite sample can be achieved, and the quality of the sample can be expected to be the best among all these methods. Table 6.1 [57] lists a brief summary to show the advantages more visualized. In the table, number 1, 2 and 3 are used to show ranks of each method in each specific aspect, where 1 represents the best case, and 3 is the worst case.

Table 6.1 Comparison of different thin film fabrication methods [57]

	Printing	Spin Coat	Painting
Material Efficiency	1	3	2
Geometry Control	1	3	2
Fabrication Speed	2	3	1
Repeatability	1	2	3
Flexibility	1	3	2
Easiness for industrial usage	1	2	3

Printing method also shows great advantages in repeatability. In another research done by Li [57], the samples of CNT-PI nanocomposites is observed under SEM and optical microscope, as shown Figure 6.1, both pictures show that the distribution of the drops are uniform and have a similar amount of the solution each drop.

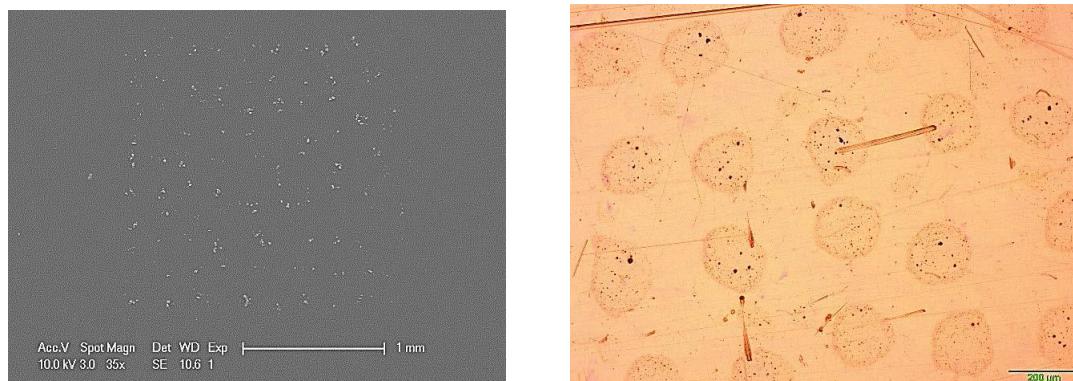


Figure 6.1 Drops of the sample under microscope [57]

6.2 GENERAL CONCLUSIONS

Inkjet printing technique is successfully implemented to fabricate graphene-PI nanocomposite thin film strain sensor, and the piezoresistive properties of the nanocomposites are characterized by tensile test and pressure test. The sensitivity of graphene-PI nanocomposites strain sensor is much higher than traditional metallic strain sensors do, the gauge factor of the nanocomposite strain sensor can be as high as around 30, while for metallic ones is only 2~5.

The graphene-PI nanocomposite with the highest sensitivity to strain was found through tensile test and pressure test. In the tensile test, continuous uniaxial load was applied on the substrate and the DC resistance variations of different graphene weight ratio in the nanocomposite was monitored, and the gauge factors were calculated. In pressure test, the

specified intensity of pressure generate a certain amount of strain, and the impedance of the nanocomposites with different graphene concentration was recorded, and the gauge factors were calculated again.

The resistance impedance increases as the strain increases in the tensile test, while in the pressure test, the resistance decreases when the pressure goes larger. But the gauge factor variation shares the same trend with respect to the concentration of graphene. The most sensitive one is the one with the largest gauge factor. It is concluded that the most sensitive nanocomposite is of 1.4wt% graphene concentration, which has a gauge factor of 29.43 in the tensile test, and 9.49 for the pressure test. Below this graphene concentration, the gauge factor increases as the concentration rises, beyond 1.4wt% the gauge factors start to drop down. At 1.6wt% of graphene, the gauge factor is relatively close to that at 1.4wt% in both tensile test and pressure test.

From the definition of the gauge factor, it should be a constant depending on the material property and the geometry change. However, the gauge factors from the tensile test and the pressure test are obviously different, though the change trend is the same. This could happen for the reason that simplifications were made when deriving the formula and the definition should be vary depending on different loading type and the different geometric shape of the transducer, so a more precise description of the piezoresistive properties of the transducers can be accomplished. The conclusion that the nanocomposite with 1.4wt% graphene concentration possesses the highest sensitivity is still valid.

Temperature has a significant effect on the performance of this piezoresistive nanocomposite strain/pressure sensors, as the temperature goes up, the resistive impedance of the nanocomposites dramatically decrease. The temperature coefficients of the nanocomposites were

determined for graphene concentration varies from 1.0wt% to 1.8wt%. Although the 1.4wt% graphene-PI nanocomposite has the highest sensitivity of strain, it is sensitive to temperature. With the temperature coefficient, a dummy gauge can be used or a circuit can be added in the testing Wheatstone bridge to compensate the temperature effect.

6.3 FUTURE WORKS

This research has proved that the graphene-PI nanocomposites strain sensor has superior sensitivity than traditional ones, it is a very promising candidate for fabricating high sensitive strain sensor and would have plenty of applications with its structural flexibility. Further works can be conducted to broaden the application of graphene-PI nanocomposite strain sensors.

The gauge factor of the graphene-PI nanocomposite strain sensors can be more specified. Though the highest gauge factor with respect to graphene concentration has been found at 1.4wt%, we found that the gauge factor is affected by the graphene concentration dramatically. Thus, gradient of the graphene concentration can be scaled down and one or two more concentration can be added between 1.4wt% and 1.6wt%. Considering the geometry effect, the formula to derive the gauge factor can be modified and improved.

In this research, the pressure is static. For future works, the respond of the graphene-PI nanocomposite sensor to dynamic pressure could be characterized. and combined with the pressure of a fluid. Also, the flowing speed can be determined with this nanocomposite sensor. Last but not least, the humidity effect on the gauge factor of this strain sensor should be evaluated.

BIBLIOGRAPHY

- [1] Figliola, Richard S., and Donald E. Beasley. "Theory and design for mechanical measurements." *Measurement Science and Technology* 12, no. 10 (2001): 1743.
- [2] Chen, Qian, Yingying Sun, Ying Wang, Hongbin Cheng, and Qing-Ming Wang. "ZnO nanowires–polyimide nanocomposite piezoresistive strain sensor." *Sensors and Actuators A: Physical* 190 (2013): 161-167.
- [3] Kon, Stanley, Kenn Oldham, and Roberto Horowitz. "Piezoresistive and piezoelectric MEMS strain sensors for vibration detection." In *The 14th International Symposium on: Smart Structures and Materials & Nondestructive Evaluation and Health Monitoring*, pp. 65292V-65292V. International Society for Optics and Photonics, 2007.
- [4] Pelrine, Ronald E., Roy D. Kornbluh, and Jose P. Joseph. "Electrostriction of polymer dielectrics with compliant electrodes as a means of actuation." *Sensors and Actuators A: Physical* 64, no. 1 (1998): 77-85.
- [5] Pan, Haibo. "Study of the Methods to Precisely Measure Strain Concentration in Welding joints Based on PSDI." Master's thesis, Harbin Institute of Technology, China, 2013.
- [6] H. Wang, Q.M. Zhang, L.E. Cross, R. Ting, C. Coughlin, K. Rittenmyer, The origins of electromechanical response in polyurethane elastomers, in: Proc. 9th IEEE ISAF, 1994, pp. 182 - 185.
- [7] Alciatore, David G., Michael B. Hestand, and David G. Alciatore. *Introduction to mechatronics and measurement systems*. Tata McGraw-Hill Education, 2007.
- [8] Shekhawat, Gajendra, Soo-Hyun Tark, and Vinayak P. Dravid. "MOSFET-embedded microcantilevers for measuring deflection in biomolecular sensors." *Science* 311, no. 5767 (2006): 1592-1595.
- [9] S.D. Senturia, *Microsystem Design*, Kluwer Academic Publishers, NY, 2000.
- [10] Wang, Yizhong, Allen X. Wang, Ying Wang, Minking K. Chyu, and Qing-Ming Wang. "Fabrication and characterization of carbon nanotube–polyimide composite based high temperature flexible thin film piezoresistive strain sensor." *Sensors and Actuators A: Physical* 199 (2013): 265-271.

- [11] Kim, Beom Joon, Houk Jang, Seoung-Ki Lee, Byung Hee Hong, Jong-Hyun Ahn, and Jeong Ho Cho. "High-performance flexible graphene field effect transistors with ion gel gate dielectrics." *Nano letters* 10, no. 9 (2010): 3464-3466.
- [12] Liu, Zunfeng, Qian Liu, Yi Huang, Yanfeng Ma, Shougen Yin, Xiaoyan Zhang, Wei Sun, and Yongsheng Chen. "Organic photovoltaic devices based on a novel acceptor material: graphene." *Advanced Materials* 20, no. 20 (2008): 3924-3930.
- [13] Han, Tae-Hee, Youngbin Lee, Mi-Ri Choi, Seong-Hoon Woo, Sang-Hoon Bae, Byung Hee Hong, Jong-Hyun Ahn, and Tae-Woo Lee. "Extremely efficient flexible organic light-emitting diodes with modified graphene anode." *Nature Photonics* 6, no. 2 (2012): 105-110.
- [14] Wang, Yu, Shi Wun Tong, Xiang Fan Xu, Barbaros Özyilmaz, and Kian Ping Loh. "Interface Engineering of Layer-by-Layer Stacked Graphene Anodes for High-Performance Organic Solar Cells." *Advanced Materials* 23, no. 13 (2011): 1514-1518.
- [15] Kim, Rak-Hwan, Myung-Ho Bae, Dae Gon Kim, Huanyu Cheng, Bong Hoon Kim, Dae-Hyeong Kim, Ming Li et al. "Stretchable, transparent graphene interconnects for arrays of microscale inorganic light emitting diodes on rubber substrates." *Nano letters* 11, no. 9 (2011): 3881-3886.
- [16] https://en.wikipedia.org/wiki/Strain_gauge
- [17] Simmons, Jr Edward E. "Explosion pressure gauge." U.S. Patent 2,327,935, issued August 24, 1943.
- [18] Ruge, Arthur C. "Strain gauge." U.S. Patent 2,350,972, issued June 6, 1944.
- [19] <http://www.sensorland.com/HowPage002.html#anchor180087>
- [20] Kuilla, Tapas, Sambhu Bhadra, Dahu Yao, Nam Hoon Kim, Saswata Bose, and Joong Hee Lee. "Recent advances in graphene based polymer composites." *Progress in polymer science* 35, no. 11 (2010): 1350-1375.
- [21] Zhang, Yuanbo, Yan-Wen Tan, Horst L. Stormer, and Philip Kim. "Experimental observation of the quantum Hall effect and Berry's phase in graphene." *Nature* 438, no. 7065 (2005): 201-204.
- [22] Miao, F., S. Wijeratne, Y. Zhang, U. C. Coskun, W. Bao, and C. N. Lau. "Phase-coherent transport in graphene quantum billiards." *Science* 317, no. 5844 (2007): 1530-1533.
- [23] Ovid'ko, I. A. "Mechanical properties of graphene." *Rev. Adv. Mater. Sci* 34 (2013): 1-11.
- [24] He, Rongrui, and Peidong Yang. "Giant piezoresistance effect in silicon nanowires." *Nature nanotechnology* 1, no. 1 (2006): 42-46.

- [25] Reck, Kasper, Jacob Richter, Ole Hansen, and Erik Vilain Thomsen. "Piezoresistive effect in top-down fabricated silicon nanowires." In *Micro Electro Mechanical Systems, 2008. MEMS 2008. IEEE 21st International Conference on*, pp. 717-720. IEEE, 2008.
- [26] Wan, Qing, Q. H. Li, Y. J. Chen, Ta-Hung Wang, X. L. He, J. P. Li, and C. L. Lin. "Fabrication and ethanol sensing characteristics of ZnO nanowire gas sensors." *Applied Physics Letters* 84, no. 18 (2004): 3654-3656.
- [27] Yu, Xun, and Eil Kwon. "A carbon nanotube/cement composite with piezoresistive properties." *Smart Materials and Structures* 18, no. 5 (2009): 055010.
- [28] Kiuchi, Mario, Shinji Matsui, and Yoshitada Isono. "The piezoresistance effect of FIB-deposited carbon nanowires under severe strain." *Journal of Micromechanics and Microengineering* 18, no. 6 (2008): 065011.
- [29] Loh, Kenneth J., Jerome P. Lynch, B. S. Shim, and N. A. Kotov. "Tailoring piezoresistive sensitivity of multilayer carbon nanotube composite strain sensors." *Journal of Intelligent Material Systems and Structures* 19, no. 7 (2008): 747-764.
- [30] Chang, Fuh-Yu, Ruoh-Huey Wang, Hsiharng Yang, Yu-Hsien Lin, Tse-Min Chen, and Shu-Jiuan Huang. "Flexible strain sensors fabricated with carbon nano-tube and carbon nano-fiber composite thin films." *Thin Solid Films* 518, no. 24 (2010): 7343-7347.
- [31] Wichmann, Malte HG, Samuel T. Buschhorn, Jan Gehrmann, and Karl Schulte. "Piezoresistive response of epoxy composites with carbon nanoparticles under tensile load." *Physical Review B* 80, no. 24 (2009): 245437.
- [32] Kim, Young-Ju, Ju Young Cha, Heon Ham, Hoon Huh, Dae-Sup So, and Inpil Kang. "Preparation of piezoresistive nano smart hybrid material based on graphene." *Current Applied Physics* 11, no. 1 (2011): S350-S352.
- [33] Hu, Ning, Yoshifumi Karube, Masahiro Arai, Tomonori Watanabe, Cheng Yan, Yuan Li, Yaolu Liu, and Hisao Fukunaga. "Investigation on sensitivity of a polymer/carbon nanotube composite strain sensor." *Carbon* 48, no. 3 (2010): 680-687.
- [34] Kang, Inpil, et al. "A carbon nanotube strain sensor for structural health monitoring." *Smart materials and structures* 15.3 (2006): 737.
- [35] Chen, Qingyun, Yuezhen Bin, and Masaru Matsuo. "Characteristics of ethylene-methyl methacrylate copolymer and ultrahigh molecular weight polyethylene composite filled with multiwall carbon nanotubes prepared by gelation/crystallization from solutions." *Macromolecules* 39, no. 19 (2006): 6528-6536.
- [36] Hsieh, Gen-Wen, Flora M. Li, Paul Beecher, Arokia Nathan, Yiliang Wu, Beng S. Ong, and William I. Milne. "High performance nanocomposite thin film transistors with bilayer carbon nanotube-polythiophene active channel by ink-jet printing." *Journal of applied physics* 106, no. 12 (2009): 123706.

- [37] Hu, Ning, Hisao Fukunaga, Satoshi Atobe, Yaolu Liu, and Jinhua Li. "Piezoresistive strain sensors made from carbon nanotubes based polymer nanocomposites." *Sensors* 11, no. 11 (2011): 10691-10723.
- [38] Jing, Zhao, Zhang Guang-Yu, and Shi Dong-Xia. "Review of graphene-based strain sensors." *Chinese Physics B* 22, no. 5 (2013): 057701.
- [39] Huang, Mingyuan, Tod A. Pascal, Hyungjun Kim, William A. Goddard III, and Julia R. Greer. "Electronic– mechanical coupling in graphene from in situ nanoindentation experiments and multiscale atomistic simulations." *Nano letters* 11, no. 3 (2011): 1241-1246.
- [40] Yu, Ting, Zhenhua Ni, Chaoling Du, Yumeng You, Yingying Wang, and Zexiang Shen. "Raman mapping investigation of graphene on transparent flexible substrate: The strain effect." *The Journal of Physical Chemistry C* 112, no. 33 (2008): 12602-12605.
- [41] Loffredo, F., A. D. G. D. Mauro, G. Burrasca, V. La Ferrara, L. Quercia, E. Massera, G. Di Francia, and D. Della Sala. "Ink-jet printing technique in polymer/carbon black sensing device fabrication." *Sensors and Actuators B: Chemical* 143, no. 1 (2009): 421-429.
- [42] Fu, Xue-Wen, Zhi-Min Liao, Jian-Xin Zhou, Yang-Bo Zhou, Han-Chun Wu, Rui Zhang, Guangyin Jing et al. "Strain dependent resistance in chemical vapor deposition grown graphene." *Applied Physics Letters* 99, no. 21 (2011): 213107.
- [43] Wijshoff, Herman. "The dynamics of the piezo inkjet printhead operation." *Physics reports* 491.4 (2010): 77-177.
- [44] Reis, Nuno, Chris Ainsley, and Brian Derby. "Ink-jet delivery of particle suspensions by piezoelectric droplet ejectors." *Journal of Applied Physics* 97, no. 9 (2005): 094903.
- [45] Singh, Madhusudan, Hanna M. Haverinen, Parul Dhagat, and Ghassan E. Jabbour. "Inkjet printing—process and its applications." *Advanced materials* 22, no. 6 (2010): 673-685.
- [46] Hilton, Ordway. *Scientific examination of questioned documents*. CRC press, 1992.
- [47] https://en.wikipedia.org/wiki/Inkjet_printing
- [48] Taylor, Geoffrey. "Disintegration of water drops in an electric field." *Proceedings of the Royal Society of London. Series A. Mathematical and Physical Sciences* 280.1382 (1964): 383-397.
- [49] Bugdayci, Nur, David B. Bogy, and Frank E. Talke. "Axisymmetric motion of radially polarized piezoelectric cylinders used in ink jet printing." *IBM Journal of Research and Development* 27.2 (1983): 171-180.

- [50] Stemme, Erik, and S-G. Larsson. "The piezoelectric capillary injector—a new hydrodynamic method for dot pattern generation." *Electron Devices, IEEE Transactions on* 20.1 (1973): 14-19.
- [51] Kyser, Edmond L., Leland F. Collins, and Nick Herbert. "Design of an impulse ink jet." *Journal of Applied Photographic Engineering* 7.3 (1981): 73-79.
- [52] Calvert, Paul. "Inkjet printing for materials and devices." *Chemistry of materials* 13, no. 10 (2001): 3299-3305.
- [53] Van Osch, Thijs HJ, et al. "Inkjet printing of narrow conductive tracks on untreated polymeric substrates." *Advanced Materials* 20.2 (2008): 343-345.
- [54] Singh, Madhusudan, Hanna M. Haverinen, Parul Dhagat, and Ghassan E. Jabbour. "Inkjet printing—process and its applications." *Advanced materials* 22, no. 6 (2010): 673-685.
- [55] Bietsch, Alexander, Jiayun Zhang, Martin Hegner, Hans Peter Lang, and Christoph Gerber. "Rapid functionalization of cantilever array sensors by inkjet printing." *Nanotechnology* 15, no. 8 (2004): 873.
- [56] het Panhuis, In. "M.; Heurtematte, A.; Small, WR; Paunov, VN Inkjet printed water sensitive transparent films from natural gum—Carbon nanotube composites." *Soft Matter* 3 (2007): 840-843.
- [57] LI, QIUYAN. "CNT-Polyimide Nanocomposite Piezoresistive Thin Film Devices for Strain and Pressure Measurement." PhD diss., University of Pittsburgh, 2015.
- [58] Ding, Tianhuai, Luheng Wang, and Peng Wang. "Changes in electrical resistance of carbon-black-filled silicone rubber composite during compression." *Journal of Polymer Science Part B: Polymer Physics* 45, no. 19 (2007): 2700-2706.
- [59] Suppression of the coffee-ring effect by shape-dependent capillary interactions. *Nature*. 2011-08-18,476.
- [60] MicroFab Techniques, Inc., Jetlab Tutorial Guide, Plano, Texas, 2006.
- [61] Bae, Sang-Hoon, Youngbin Lee, Bhupendra K. Sharma, Hak-Joo Lee, Jae-Hyun Kim, and Jong-Hyun Ahn. "Graphene-based transparent strain sensor." *Carbon* 51 (2013): 236-242.